954795

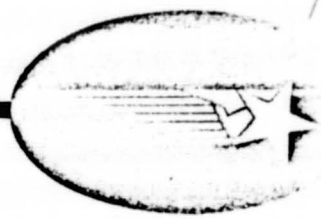

MARS ROVER SYSTEM
LOOPWHEEL DEFINITION
SUPPORT

October 1977

Final

(NASA-CR-157085) MARS ROVER SYSTEM LOOPWHEEL DEFINITION SUPPORT Final Report (Lockheed Missiles and Space Co.) 86 p
HC A05/MF A01 CSCL 13I

N78-24253

Unclas
G3/14 20712

Lockheed

HUNTSVILLE RESEARCH & ENGINEERING CENTER

LOCKHEED MISSILES & SPACE COMPANY, INC.
A SUBSIDIARY OF LOCKHEED AIRCRAFT CORPORATION

HUNTSVILLE, ALABAMA

Lockheed

Missiles & Space Company, Inc.

HUNTSVILLE RESEARCH & ENGINEERING CENTER

Cummings Research Park
4800 Bradford Drive,
Huntsville, Alabama

MARS ROVER SYSTEM LOOPWHEEL DEFINITION SUPPORT

October 1977

Contract No. 954795

Jet Propulsion Laboratory
Pasadena, California 91103

by

Wolfgang Trautwein

APPROVED: B. Hobson Shirley

B. Hobson Shirley, Supervisor
Engineering Sciences Section

J.S. Farrior

J.S. Farrior
Resident Director

FOREWORD

This report documents the results of work under Contract JPL 954795 to support the Jet Propulsion Laboratory in defining the traction elements for JPL's point design Mars Rover utilizing Lockheed's loopwheel concept. The JPL Technical Manager was Mr. J.R. French.

The work was performed by personnel of Lockheed Missiles & Space Company's Huntsville Research & Engineering Center in the Engineering Sciences Section supervised by Mr. B. Hobson Shirley. Dr. Wolfgang Trautwein was the Project Engineer.

PROPRIETARY NOTICE

Section 1
INTRODUCTION AND SUMMARY

Lockheed Missiles & Space Company's Huntsville Research & Engineering Center has for the last seven years developed the loopwheel (or Elastic Loop) mobility concept, which appears to be uniquely qualified to provide a high degree of mobility at low weight and stowage requirements for the next Mars mission now in the early planning stage.

The development of the loopwheel mobility concept was initiated at Lockheed-Huntsville in 1969 as a Company-funded project and has received continued Company support to this date. A first generation test unit was completed in 1970 under Lockheed's Independent Development Program.

NASA-Marshall Space Flight Center supported the exploratory development for low-gravity extraterrestrial applications from 1970 to 1973 through several prototype and test programs. Tests of a second generation loopwheel were conducted for NASA by the U.S. Army Engineer Waterways Experiment Station (WES) in Vicksburg, Mississippi. These tests have shown that the loopwheel provides an 85 to 100% improvement in soft soil traction over the wheeled Lunar Roving Vehicle at lower power requirements.

The objective of this study effort was to support the JPL in defining the mobility system for JPL's point design Mars Rover.

Loopwheel traction elements were designed which are compatible with the specified rover mass, range and stowage requirements (Fig. 1-1). Additional volume for stowing deployable science or other subsystems within the loopwheel envelopes has been incorporated (Fig. 1-2). Any such equipment which can be located inside the loopwheel trucks improves the rover's static stability and overall mobility and reduces the overall stowed volume of the rover within the aeroshell.

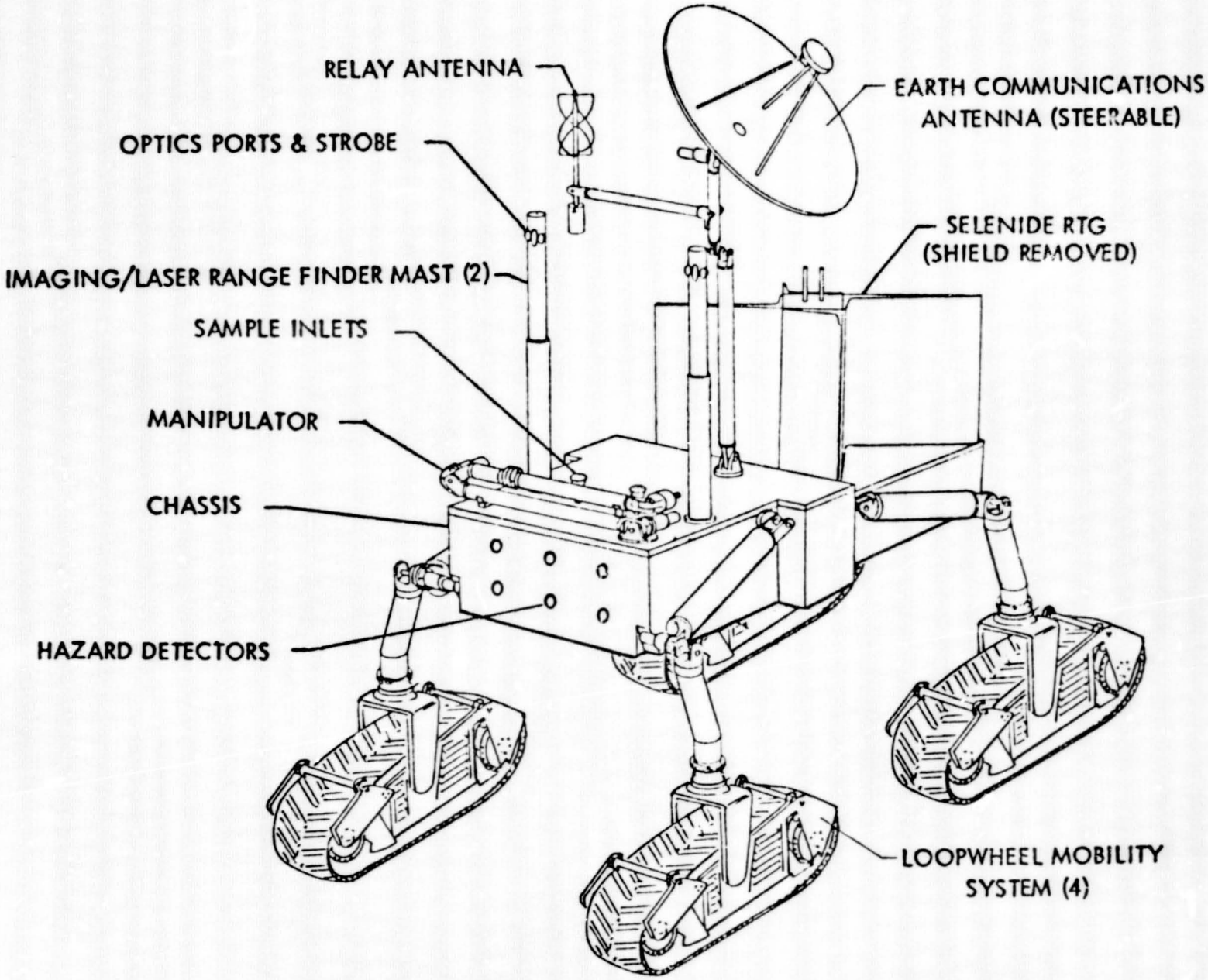

Fig. 1-1 - Mars Rover Point Design (Jointed Suspension Option) with Loopwheel Mobility System.

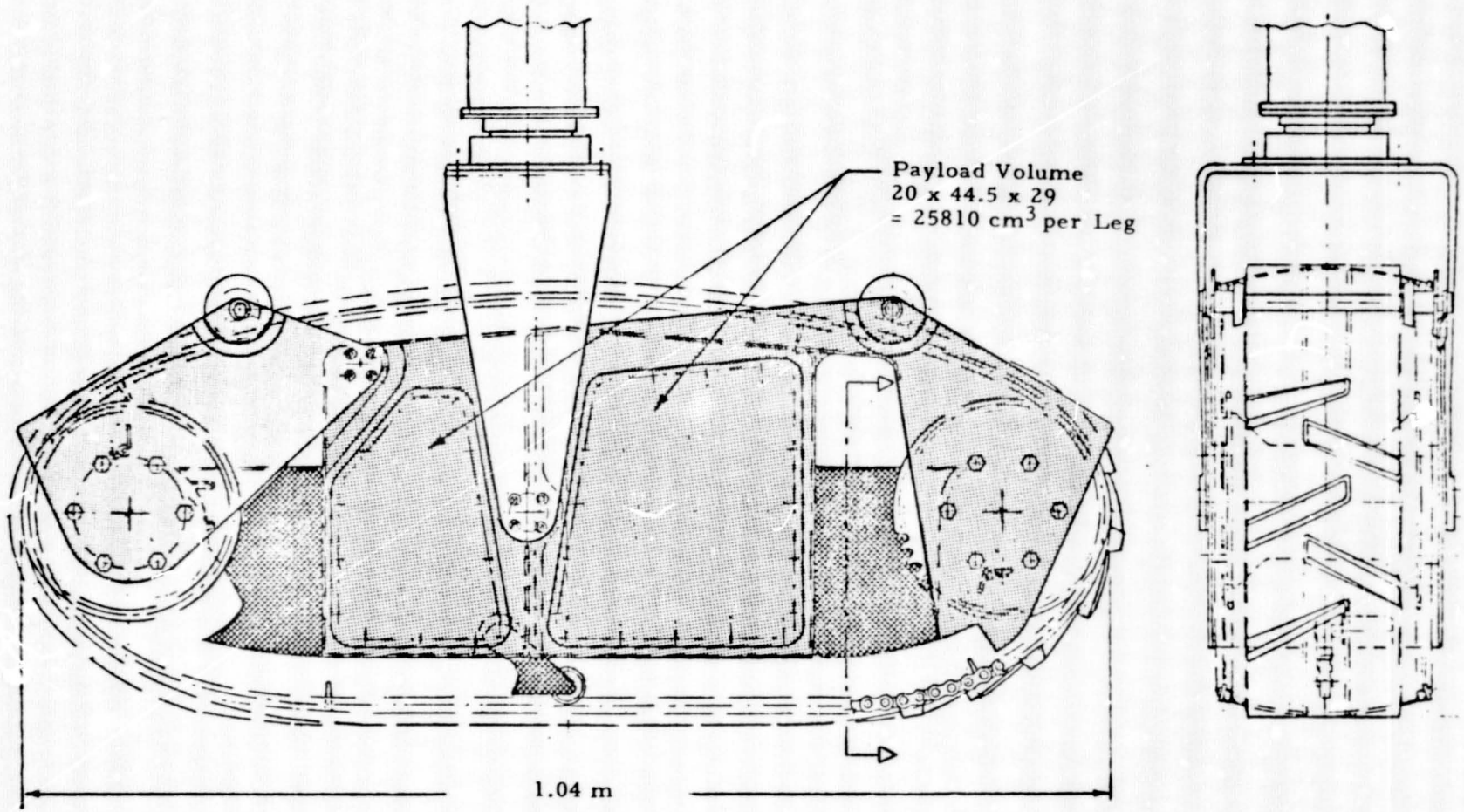

Fig. 1-2 - Loopwheel Mobility System with Integral Payload Bays and Rock Removal System

The recent development and laboratory testing of a loopwheel suspension of similar size (1.27 m O.A. length) for the U.S. Army Tank Automotive Research & Development Command (Fig. 1-3) proved to be a valuable aid in the prediction of traction element mass and performance characteristics.

Four steering concepts were evaluated. An optimum concept was identified on the basis of maximum probability of mission success. In the structural analysis of the loopwheel core and tread as the major fatigue critical components, important technology areas were identified which should be addressed early in the rover development. A reliable assessment of the rover's operational and science-oriented mission capabilities requires testing of a full-size functional rover test article.

On the basis of the design and analysis efforts to date and of on-going loopwheel hardware programs, the present rover point design can be expected to provide excellent mobility at light weight and high efficiency far exceeding the LRV capabilities in soil conditions ranging from low strength Loess to boulder-strewn regions. State-of-the-art material technology appears sufficient to achieve a 500 km design life of the traction elements on Mars.

Continuing SRT efforts in selected critical manufacturing and test areas are recommended in Section 4 which promise to substantially reduce future development risks and cost.

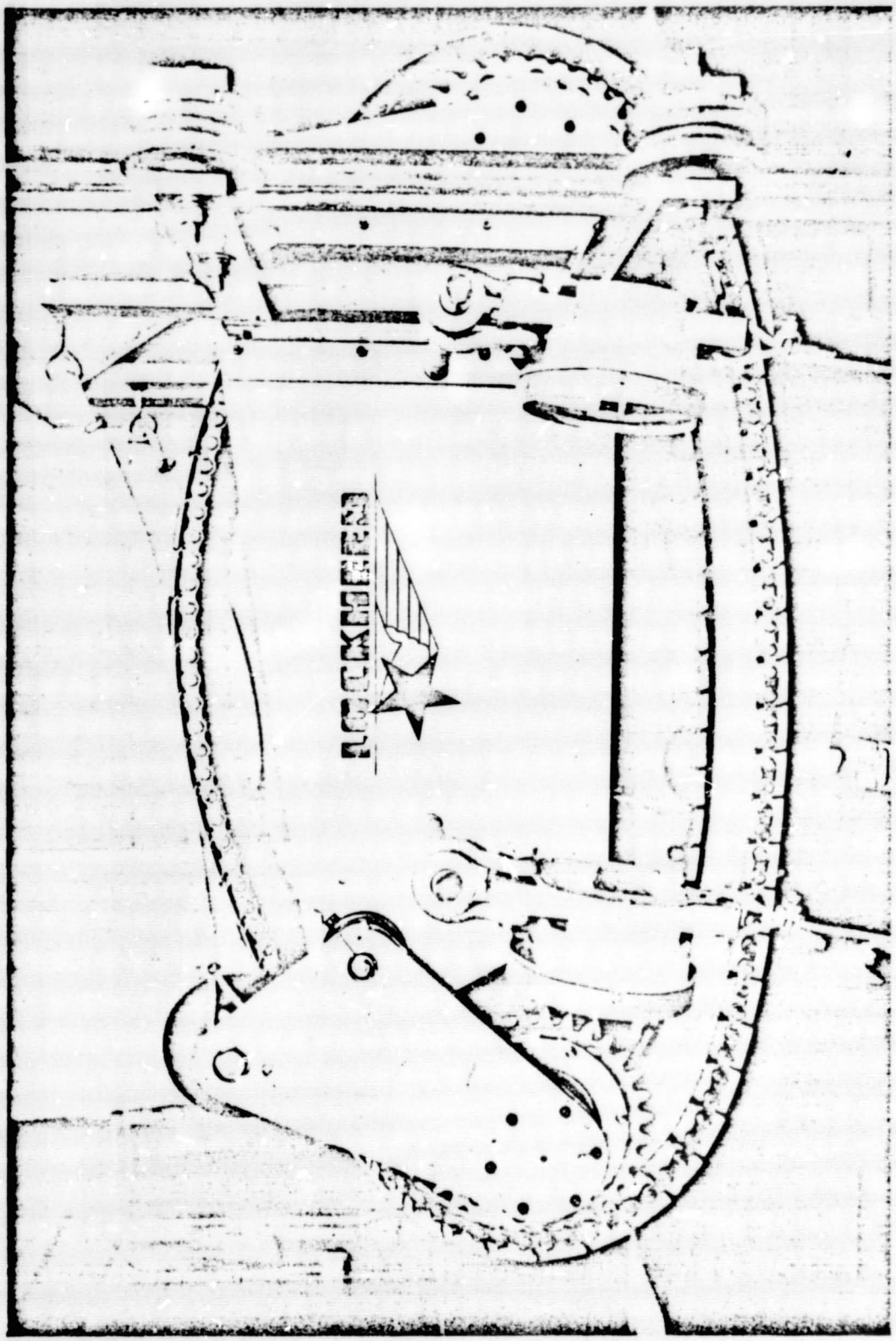

Fig. 1-3 - Operational Loopwheel Suspension Developed and Tested Recently for the Army Tank Automotive Research and Development Command Provided Realistic Mass and Performance Data Due to Its Similar Size (1.27 m O.A. length) (Ref. 1)

Section 2
TRACTION ELEMENT ANALYSIS AND DESIGN

2.1 WORST CASE LOAD CONDITIONS

2.1.1 Selection of Rover Suspension Systems for Analysis

The major deviations from the static load distribution among the four loopwheels will occur when slopes are negotiated. The uphill loopwheels will be partially off-loaded, and increasing loads will be transferred to the downhill loopwheels. The magnitude of load transfer on a given slope depends strongly on the center-of-mass location and on the kinematics of the vehicle suspension.

In order to determine the worst case loads that a rover traction element may have to support, an analysis was performed for two suspension options of the JPL point design. Both of these options feature free rotation in pitch for all four loopwheels.

In the first option all four pitch pivot points were assumed to be rigidly connected to the rover chassis (not considering steering), whereas in the second option the two front pitch pivot points were assumed to be at the outer ends of a front axle which has a roll degree of freedom with respect to the rover chassis (Fig. 2-1, from Ref. 3).

2.1.2 Load Transfer for Option I: Front and Rear Suspension Without Roll Degrees of Freedom

Figure 2-2 shows a schematic representation of the rover. It defines the static forces, the dimensional parameters and a body-fixed coordinate system (subscript V).

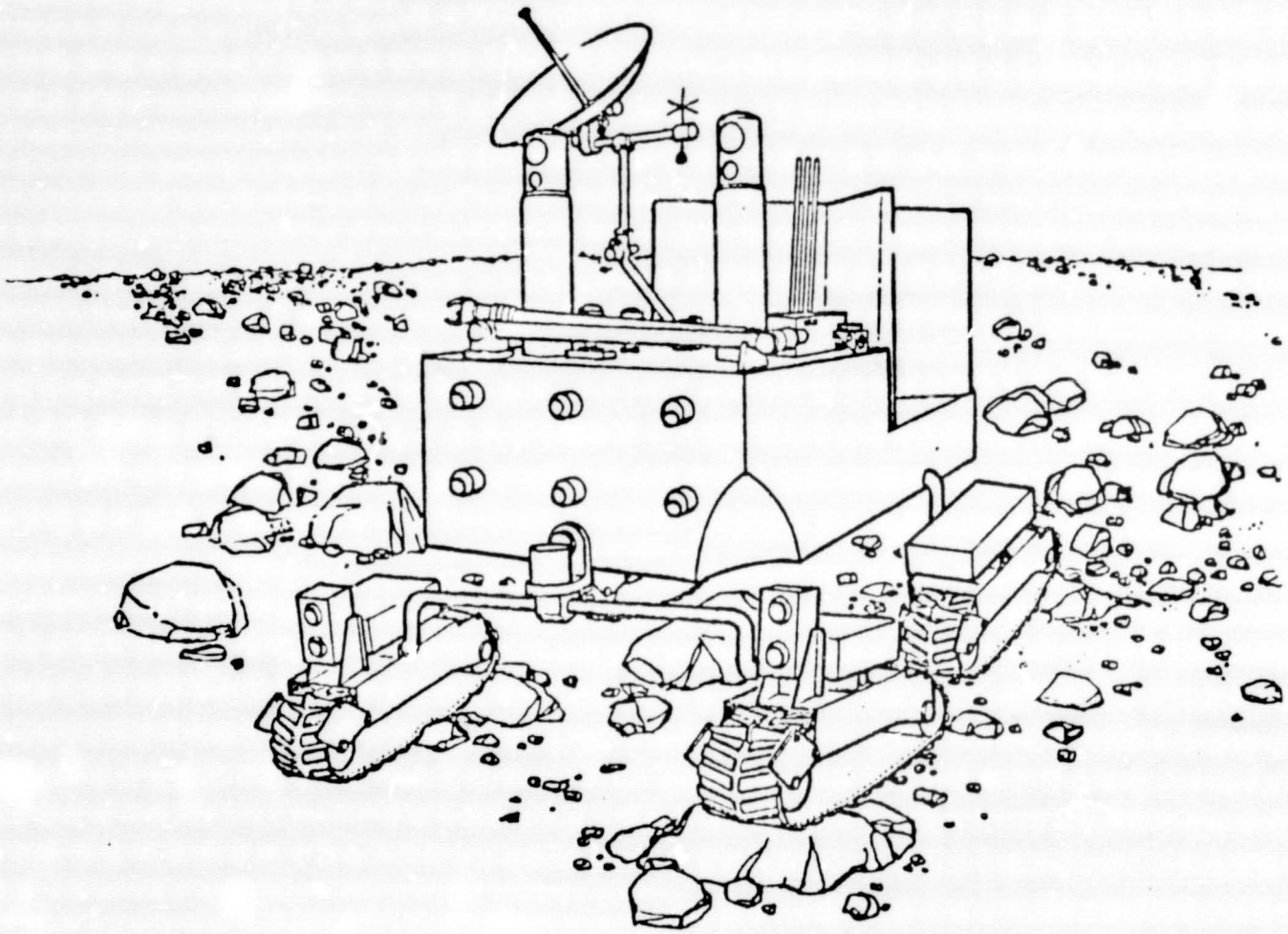

Fig. 2-1 - Suspension Option II (Front Axle Pivoted in Roll)

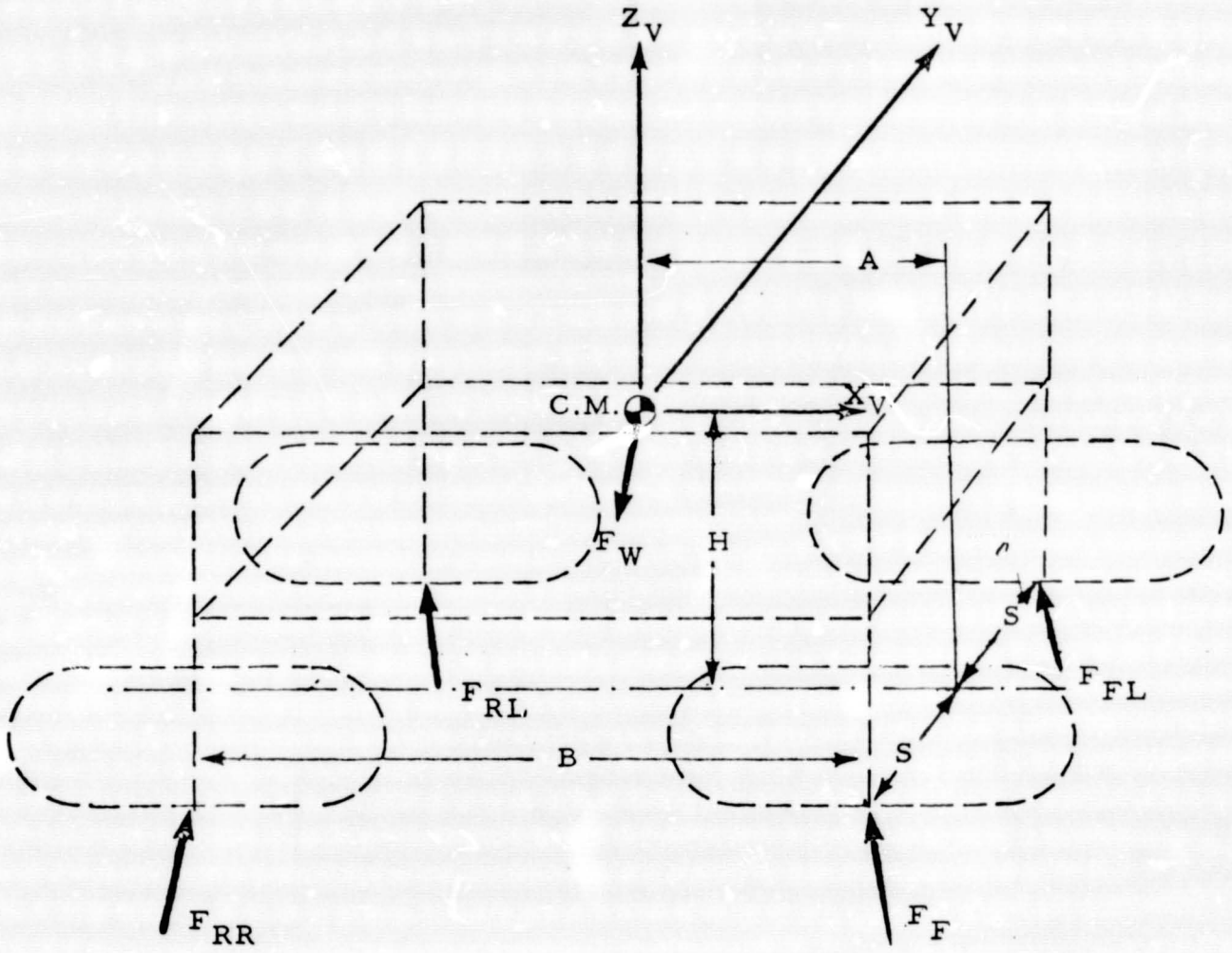

Fig. 2-2 - Notations for Suspension Option I

The force and moment equations for static equilibrium are as follows:

$$F_{RRX} + F_{RLX} + F_{FRX} + F_{FLX} + F_{WX} = 0 \quad (1)$$

$$F_{RRY} + F_{RLY} + F_{FRY} + F_{FLY} + F_{WY} = 0 \quad (2)$$

$$F_{RRZ} + F_{RLZ} + F_{FRZ} + F_{FLZ} + F_{WZ} = 0 \quad (3)$$

$$(F_{RLZ} - F_{RRZ} + F_{FLZ} - F_{FRZ})S + (F_{RRY} + F_{RLY} + F_{FRY} + F_{FLY})H = 0 \quad (4)$$

$$(F_{RRZ} + F_{RLZ})(B-A) - (F_{FRZ} + F_{FLZ})A - (F_{RRX} + F_{RLX} + F_{FRX} + F_{FLX})H = 0 \quad (5)$$

$$(F_{RRX} - F_{RLX} + F_{FRX} - F_{FLX})S - (F_{RRY} + F_{RLY})(B - A) + (F_{FRY} + F_{FLY})A = 0 \quad (6)$$

To determine the worst case loads it was assumed that the rover is crossing a sloping uneven terrain such that one of the loops is completely unloaded. As a worst case it was assumed that one of the rear loops is unloaded while the rover climbs a combination of forward and side slopes. The derivation presented here assumes that the left rear loop carries no load, i.e.,

$$F_{RLX} = F_{RLY} = F_{RLZ} = 0$$

Furthermore, some relationship must be assumed among the forces parallel to the surface. The relationship selected is the requirement that the traction and side load forces are proportional to the normal forces. Specifically,

$$F_{RRX} = \mu_X F_{RRZ}$$

$$F_{FRX} = \mu_X F_{FRZ}$$

$$F_{FLX} = \mu_X F_{FLZ}$$

$$F_{FRY} = \mu_Y F_{FRZ}$$

$$F_{FLY} = \mu_Y F_{FLZ}$$

where μ_X and μ_Y are longitudinal and lateral coefficients of friction.

The set of algebraic equations may now be solved. This results in the following normal forces for the three load carrying loopwheels:

$$F_{FRZ} = F_{WX} \frac{H}{B} - F_{WY} \frac{H}{2S} + F_{WZ} \left(\frac{A}{B} - \frac{1}{2}\right)$$

$$F_{FLZ} = F_{WY} \frac{H}{2S} - \frac{1}{2} F_{WZ}$$

$$F_{RRZ} = -F_{WY} \left(\mu_X \frac{H}{S} + A\right) \frac{1}{B}$$

$$\mu_X = \frac{F_{WX}}{F_{WZ}}$$

2.1.3 Load Transfer for Option II: Roll DOF Between Front and Rear Suspension

A schematic representation of the rover with a pivoted front axle is shown in Fig. 2-3. The figure defines the forces, the dimensional parameters and a body fixed coordinate system. The force and moment equations for static equilibrium are listed below:

Front Axle:

$$F_{FRX} + F_{FLX} + F_{WFX} - F_{FX} = 0$$

$$F_{FRY} + F_{FLY} + F_{WFY} - F_{FY} = 0$$

$$F_{FRZ} + F_{FLZ} + F_{WFZ} - F_{FZ} = 0$$

$$(F_{FLZ} - F_{FRZ})S + (F_{FLY} + F_{FRY})C + F_{WFY}(C-D) = 0$$

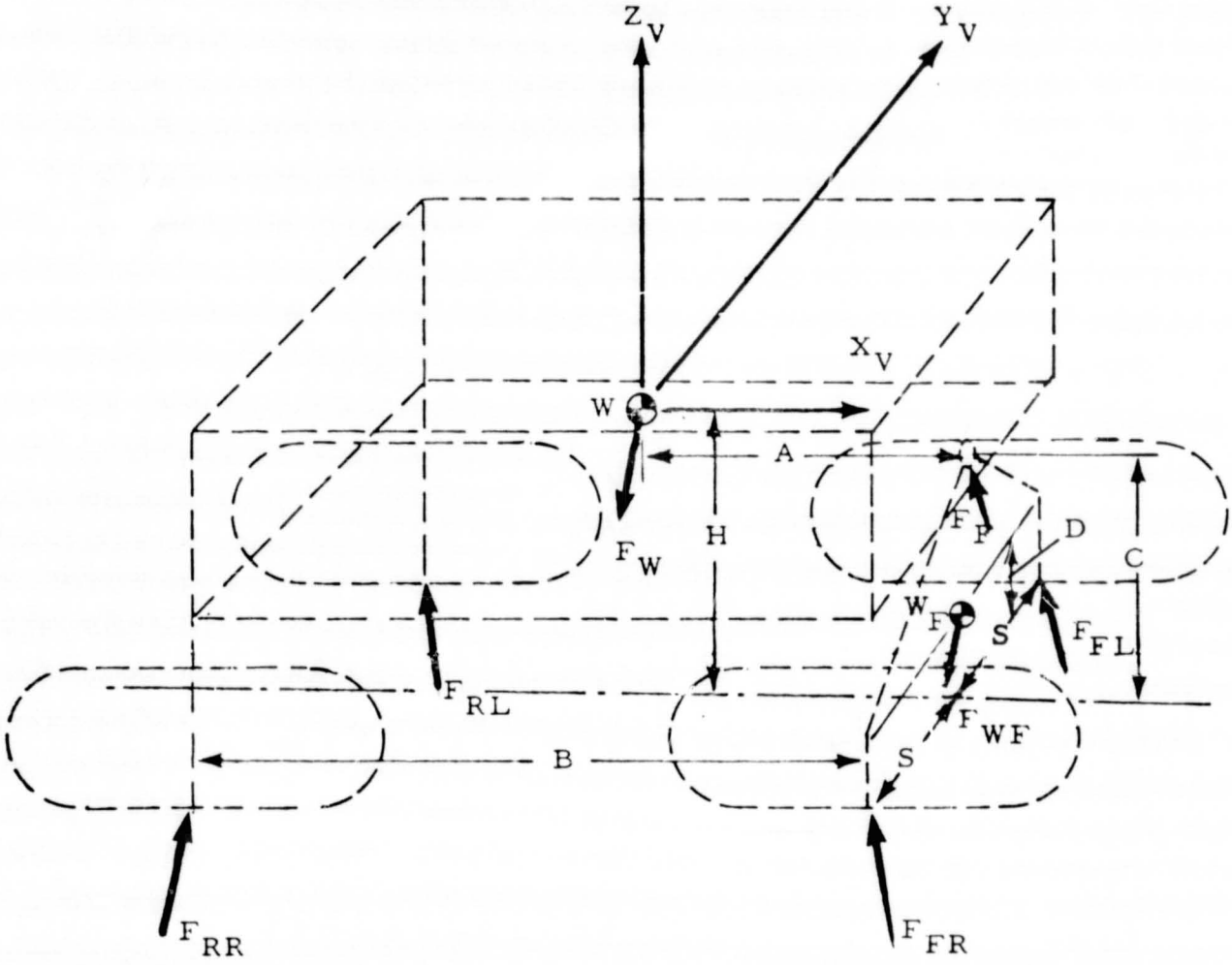

Fig. 2-3 - Notations for Pivoted Front Axle

Main Body:

$$F_{RRX} + F_{RLX} + F_{FX} + F_{WX} = 0$$

$$F_{RRY} + F_{RLY} + F_{FY} + F_{WY} = 0$$

$$F_{RRZ} + F_{RLZ} + F_{FZ} + F_{WZ} = 0$$

$$(F_{RLZ} - F_{RRZ})S + (F_{RRY} + F_{RLY})H + F_{FY}(H-C) = 0$$

$$(F_{RRZ} + F_{RLZ})(B-A) - (F_{RRX} + F_{RLX} + F_{FRX} + F_{FLX})H$$
$$- (F_{FRZ} + F_{FLZ} + F_{WFZ})A - F_{WFX}(H-D) = 0$$

$$(F_{RRX} + F_{FRX} - F_{RLX} - F_{FLX})S + (F_{FRY} + F_{FLY} + F_{WFY})A$$
$$- (F_{RRY} + F_{RLY})(B-A) = 0$$

As in the case with the fixed front axle, it is again assumed that the forces parallel to the surface are proportional to the normal forces. Specifically,

$$F_{RRX} = \mu_X F_{RRZ} \qquad F_{RRY} = \mu_{RY} F_{RRZ}$$

$$F_{RLX} = \mu_X F_{RLZ} \qquad F_{RLY} = \mu_{RY} F_{RLZ}$$

$$F_{FRX} = \mu_X F_{FRZ} \qquad F_{FRY} = \mu_{FY} F_{FRZ}$$

$$F_{FLX} = \mu_X F_{FLZ} \qquad F_{FLY} = \mu_{FY} F_{FLZ}$$

where μ_X, μ_{RY}, μ_{FY} are longitudinal and lateral coefficients of friction, respectively.

Solving the resulting set of equations yields the following expressions for the normal forces at the four loops:

$$F_{RRZ} = -F_{WX}\frac{H}{2B} - F_{WFX}\frac{D}{2B} + \left[F_{WY}(-H\mu_X - \frac{HB}{C} + B - A) - F_{WFY}\mu_X D\right]\frac{C}{2SB} - F_{WZ}\frac{A}{2B}$$

$$F_{RLZ} = -F_{WX}\frac{H}{2B} - F_{WFX}\frac{D}{2B} - \left[F_{WY}(-H\mu_X - \frac{HB}{C} + B - A) - F_{WFY}\mu_X D\right]\frac{C}{2SB} - F_{WZ}\frac{A}{2B}$$

$$F_{FLZ} = F_{WX}\frac{H}{2B} + F_{WFX}\frac{D}{2B} + F_{WY}\frac{C}{2BS}(-H\mu_X + B - A) - F_{WFY}\frac{D}{2S}(\frac{\mu_X C}{B} - 1) - F_{WZ}\frac{B-A}{2B} - F_{WFZ}\frac{1}{2}$$

$$F_{FRZ} = F_{WX}\frac{H}{2B} + F_{WFX}\frac{D}{2B} - F_{WY}\frac{C}{2BS}(-H\mu_X + B - A) + F_{WFY}\frac{D}{2S}(\frac{\mu_X C}{B} - 1) - F_{WZ}\frac{B-A}{2B} - F_{WFZ}\frac{1}{2}$$

$$\mu_X = \frac{F_{WX} + F_{WFX}}{F_{WZ} + F_{WFZ}}$$

2.1.4 Terrain Slope and Direction of Travel

The load transfer to the four loopwheels was studied for the rover climbing a combination of forward and side slopes. The terrain slope, α, and the direction of travel, ψ, of the rover are depicted in Fig. 2-4. The reference coordinate system X_I-Y_I-Z_I points with the Z_I axis along the local vertical. The plane X'_I-Y'_I represents the terrain surface with a slope α. The rover fixed coordinate system X_V-Y_V-Z_V points with the X_V axis in the direction of travel, which is defined by the angle ψ.

The transformation matrix from the reference to the rover fixed coordinate system is

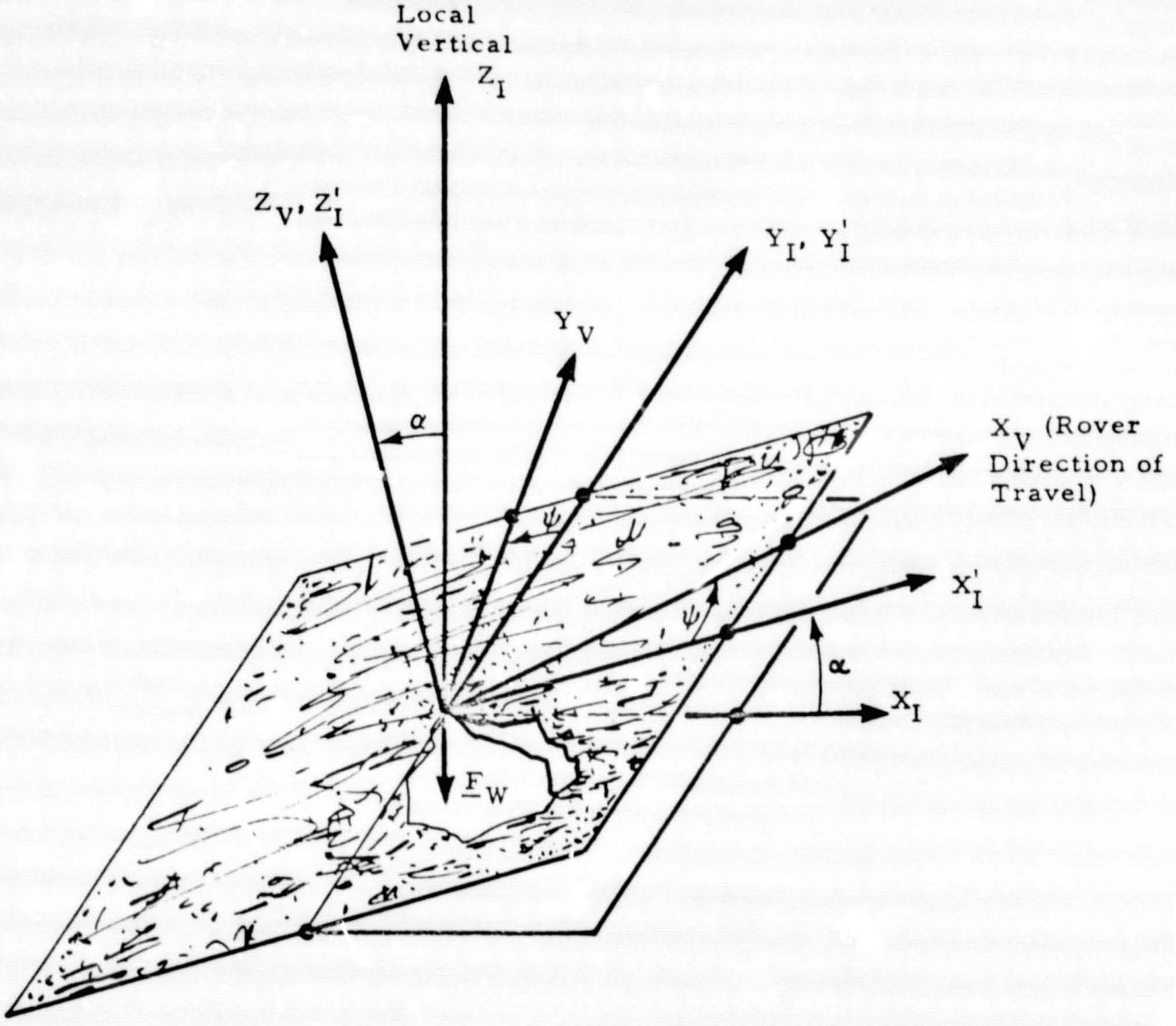

Fig. 2-4 - Definition of Terrain Slope and Direction of Travel

$$T_{VI} = \begin{bmatrix} C\psi\, C\alpha & S\psi & C\psi\, S\alpha \\ -S\psi\, C\alpha & C\psi & -S\psi\, S\alpha \\ -S\alpha & 0 & C\alpha \end{bmatrix}, \text{ where } \begin{array}{l} C = \cos \\ S = \sin \end{array}$$

The weight vector $\underline{F}_W$ can now be expressed in the rover fixed coordinate system by

$$\underline{F}_W^V = T_{VI}\, \underline{F}_W^I = \begin{bmatrix} -C\psi\, S\alpha \\ S\psi\, S\alpha \\ -C\alpha \end{bmatrix} W$$

where W is the rover weight on Mars, mg_{σ} ($g_{\sigma} = 3.75\ m/sec^2$).

2.1.5 Effect of Loopwheel Spring Deflection

The expressions derived above for the loop loads do not account for the additional shift in load due to the varying amounts of spring deflection of the four loops which will increase the tilt of the chassis, thereby increasing the load shift from uphill to downhill loops.

A reasonably accurate representation of loopwheel spring deflection is obtained by assuming a linear spring with finite travel between hard stops built into the suspension. This is a nonlinear representation which makes it difficult to obtain closed form solutions. An iterative procedure was therefore developed, which consists of the following steps:

1. Compute loads for rigid suspension as derived for Case 1 or Case 2.
2. Compute compression (or expansion) of loops based on linear spring model with finite travel.
3. Compute additional tilt of rover body due to loop compression.
4. Compute new direction of weight vector, F_W, based on terrain slope and body tilt of Step 3.
5. Go to Step 1.

This iterative procedure was implemented in a computer program. It converged to five significant figures within less than ten iterations.

2.1.6 Maximum Normal Loads

The subsystems of the rover point design of Ref. 3 were placed as called out in Table 1 and illustrated in Fig. 2-5. An earlier cursory analysis indicated potential stability problems in slope climbing due to a high center-of-mass location. In this detailed analysis an effort was therefore made to move the center of mass as low as possible. The payload bays inside each loopwheel truck lend themselves to placement of equipment and science packages very close to the ground. Any mass placed into these payload bays greatly enhances the rover's static stability and overall mobility characteristics. The proximity of these bays to the ground makes them the preferred locations for deployable science, drilling and active seismic equipment. It was therefore assumed that a total mass equivalent to one-third of the science allocation can be stowed inside the four loopwheel truck structures.

The results of the load transfer analysis are plotted in Fig. 2-6 for slopes of 20 and 25 deg. The penalties associated with suspension Option I without roll degree of freedom between front and rear end are substantial. Loads may exceed 2.6 times static load for the downhill loopwheel under worst case conditions of approximately 42 deg. azimuth and one loopwheel off the ground due to local terrain waviness. In suspension Option II, the roll articulation between front and rear loops reduces worst case loads to approximately two times static loads since loads are distributed to all four loopwheels at all times. An assumed total spring travel of 7.5 cm adds approximately 50 N or 11% of static load to worst case loads. A check of minimum loads on uphill loops shows that Option I is operating close to the stability limit on the 25 deg. slope, since only 26% of static load is left on the least loaded uphill loop. Such a drastic load shift would also impair steering response and is therefore undesirable.

Table 1

ROVER MASS SUMMARY (Ref. 3) WITH ASSUMED CENTER-OF-MASS LOCATIONS DEPICTED IN FIG. 2-5

Subsystem/Instrument Name	Mass (kg)	Location No. in Fig. 2-5
System	478.6	
Structure	58.5	I
Radio Frequency	9.4	V
Telemetry Modulation	2.2	V
Electrical Power	61.2	II
Data Handling and Control	35.0	V
Mobility	105.5	VII & VIII
Pyrotechnics	TBS	
Cabling	8.0	I
Temperature Control	33.5	I
Mechanical Devices	7.1	I
Manipulation	18.0	III
Antenna Pointing	4.1	VI
Data Storage	10.0	V
Antennas	20.0	VI
Active Seismic Source	*	
Electromagnetic Sounding	*	
Gamma Ray Spectrometer	*	
Reflectance Spectrometer	*	
Alpha/Proton/X-Ray Spectrometer	*	
Visual Imaging	10.0	VI
Imaging Microscopy	*	
Mass Spectrometer/Chemistry	*	
X-Ray Diffractometer	*	
Auxiliary Sample Acquisition	*	
Sample Handling	*	
Drilling	*	
Relay Radio	7.7	V
Relay Telemetry Modulation	4.4	V
Deployable Science Package	*	
	17.5	VII
* In Science Allocation of 104 kg	17.5	VIII
	69.0	IV

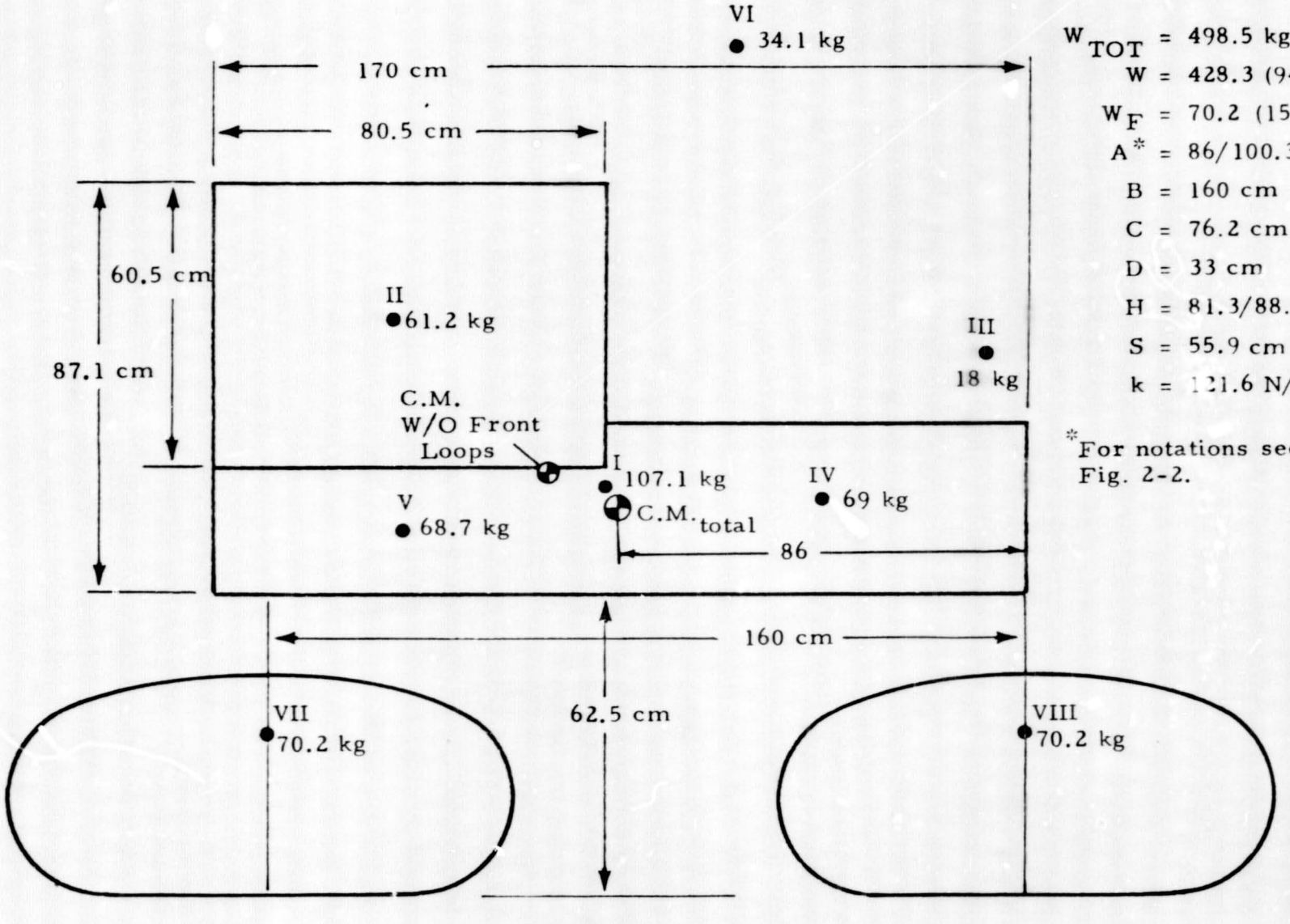

Fig. 2-5 - Mass Distribution Assumed for Load Transfer Analysis with 1/3 of Science Located Inside Loops (Subsystems are listed in Table 1)

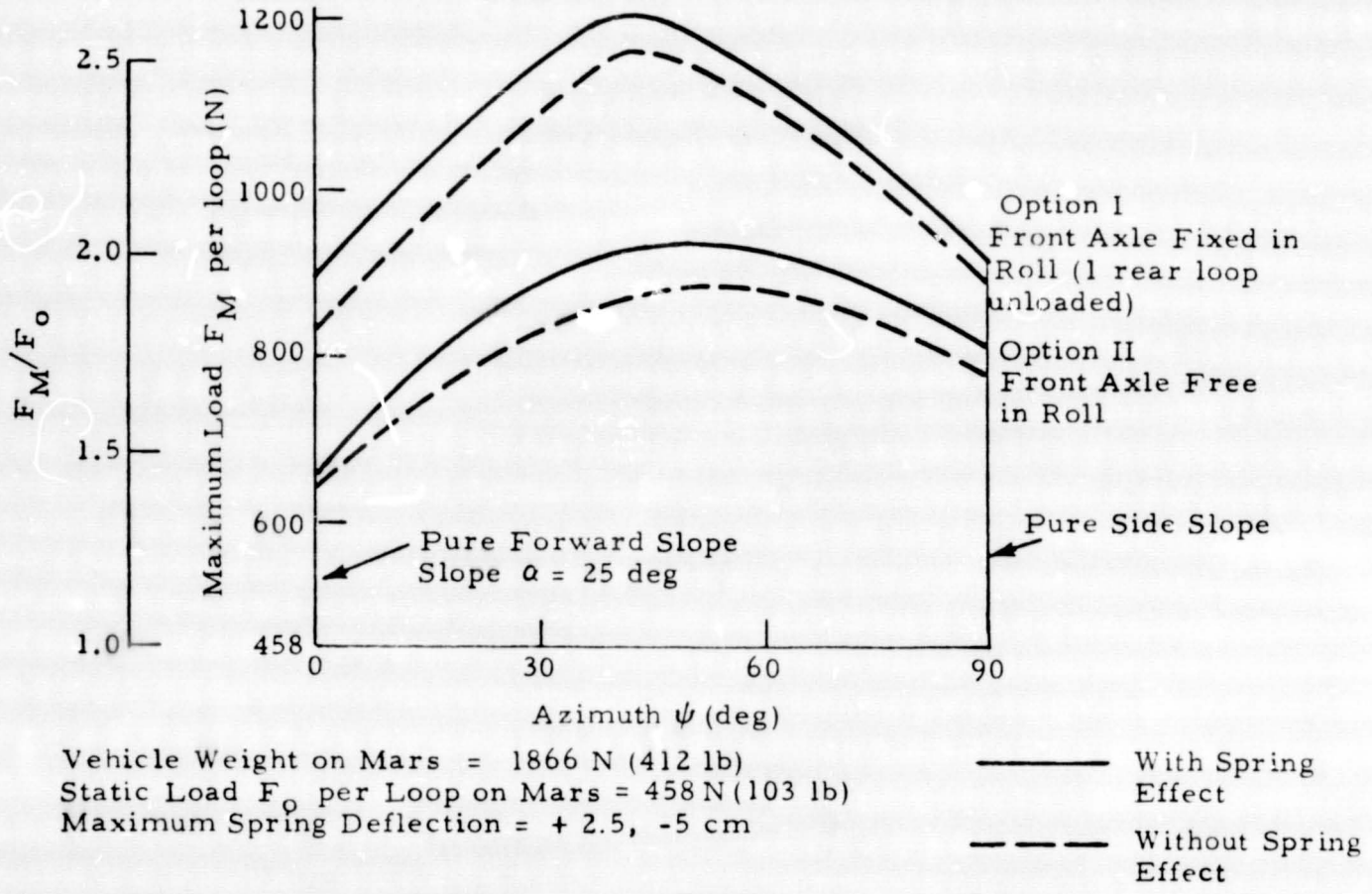

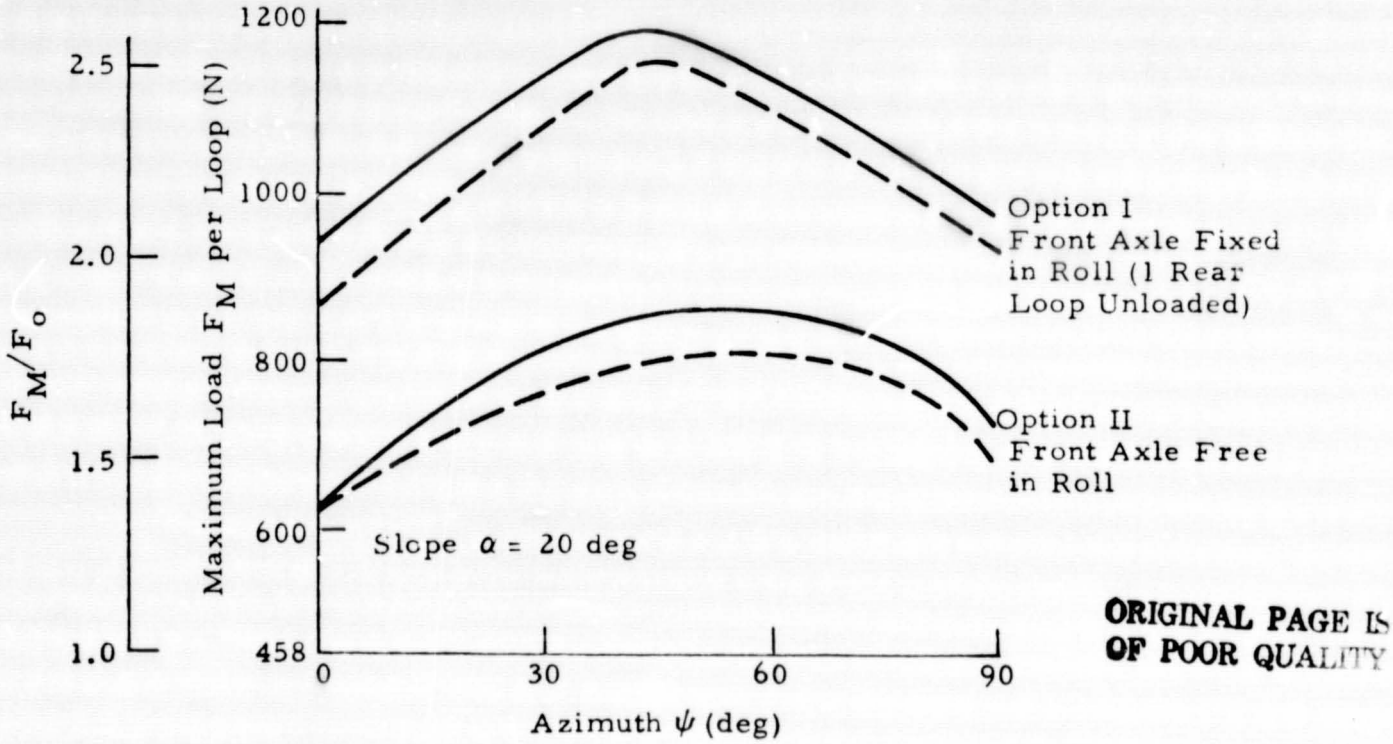

ORIGINAL PAGE IS OF POOR QUALITY

Fig. 2-6 - Maximum Load Transfer During Slope Climbing of Point Design Rover (Ref. 3)

2.1.7 Maximum Side Loads

The loopwheel suspension must be designed to transfer side loads exceeding the maximum anticipated levels from the ground to the main chassis without disengagement of sprockets from the loopwheel.

As the rover negotiates a terrain slope, α, as shown in Fig. 2-4, side loads increase monotonically as the rover steers away from the slope and reach a maximum for $|\psi| = 90$ deg when the rover moves parallel to the slope. In this case the side load, F'_S, acting on a loop is

$$F'_S = F_N \tan\alpha$$

Scuff steering may be applied either as primary or as backup emergency mode. The additional side load on each loopwheel during scuffing on level ground is

$$F_{SC} = \frac{WS}{2B} \left(\frac{F_x}{W}\right),$$

where S and B are defined in Fig. 2-3 and F_x/W is the pull coefficient (total traction in x-direction w. r. to rover weight. For the present design (S = 0.56 m, B = 1.6 m) and a maximum pull coefficient on Mars $F_x/W = 0.6$, the side load per loopwheel due to scuff steering is

$$F_{SC} = \frac{1866 \times 0.56}{2 \times 1.6} 0.6 = 196 \text{ N}$$

For the two suspension options and the maximum normal loads per loop F_N plotted in Fig. 2-6, the following side load extremes are then obtained for side slope traverses ($\psi = 90$ deg, effect of spring deflection included) and simultaneous scuff steering.

Suspension Options	Slope α (deg)	F_N	F_S	F_{Scuff}	$(F_S+F_{Scuff})/F_N$
I (No Roll)	20	980 N	357 N	196 N	0.564
II (Free Roll)	20	720 N	262 N	↓	0.636
I	25	920 N	429 N	↓	0.679
II	25	820 N	382 N	↓	0.705 = max

For design purposes it will be specified that sprocket/loopwheel engagement is maintained for

$$\frac{F_S}{F_N} = 1.25 \left(\frac{F_S}{F_N}\right)_{max} = 0.88$$

This corresponds to a 41 deg side slope or could be reached if one of the loops hits a rock as the rover skids sideways. As will be shown in Section 3 the loopwheel suspension system can tolerate temporary side loads which exceed the design allowables without damage. A higher shock load and/or safety factor above 1.25 is therefore not necessary.

2.2 FOOTPRINT REQUIREMENTS BASED ON MARS SOIL CONDITIONS

Available data on the soil properties found at the Viking 1 and Viking 2 landing sites (Refs. 4 and 5) were compared with test soils used during the Lunar Roving Vehicle (LRV) development (Ref. 6) and for performance tests of early loopwheel test articles for NASA (Ref. 7).

The results of this comparison are plotted in Figs. 2-7 through 2-9. Grain size of the test soil matches well the Viking 1 findings for the Sandy Flats which has the lowest bearing strength. The grain size distribution of the Rocky Flats regions at the Viking 1 site is coarser by a factor of 3 to 10. However, the higher strength of that soil makes it less important for traction element design.

Penetration resistance gradients of Fig. 2-8 seem also in satisfactory agreement. The major discrepancies between the test soils and the soft Viking 1 soil are density, angle of internal friction and bearing strength as shown in Figs. 2-9 and 2-10. In the worst case, angle of internal friction may be as low as 20 deg and bulk density as low as 1 g/cm^3 according to the Viking 1 observations which is in close agreement with the worst case loess properties of Ref. 8 (1 g/cm^3 density, 25 deg angle of internal friction) which are plotted in Fig. 2-10. Only for very low ground contact pressures of 0.39 N/cm^2 (0.56 psi) is there good agreement between the loosest test soil LSS1 and loess bearing strength and resulting sinkage.

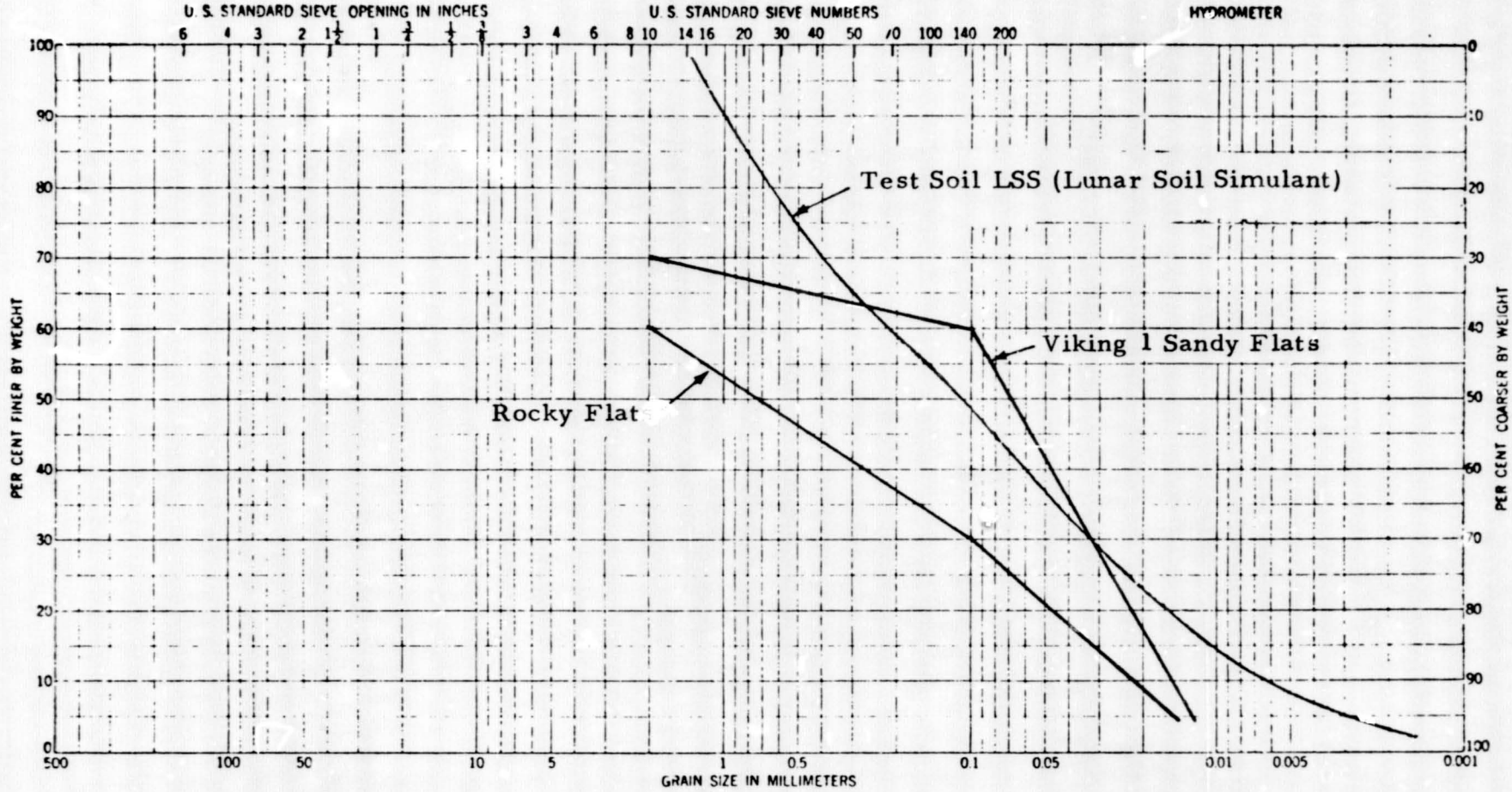

C_u: 33.00 e_{max}: 1.116 D': 2.10

d_{50}: 0.11 mm e_{min}: 0.360 γ_s: 2.85 g/cm^3

Fig. 2-7 - Gradation and Classification Data for Test Soil LSS1 through LSS5 Used in LRV and Loopwheel Performance Evaluation (Ref. 7) Compared with Martian Soil from Viking 1 Landing Site (Ref. 4)

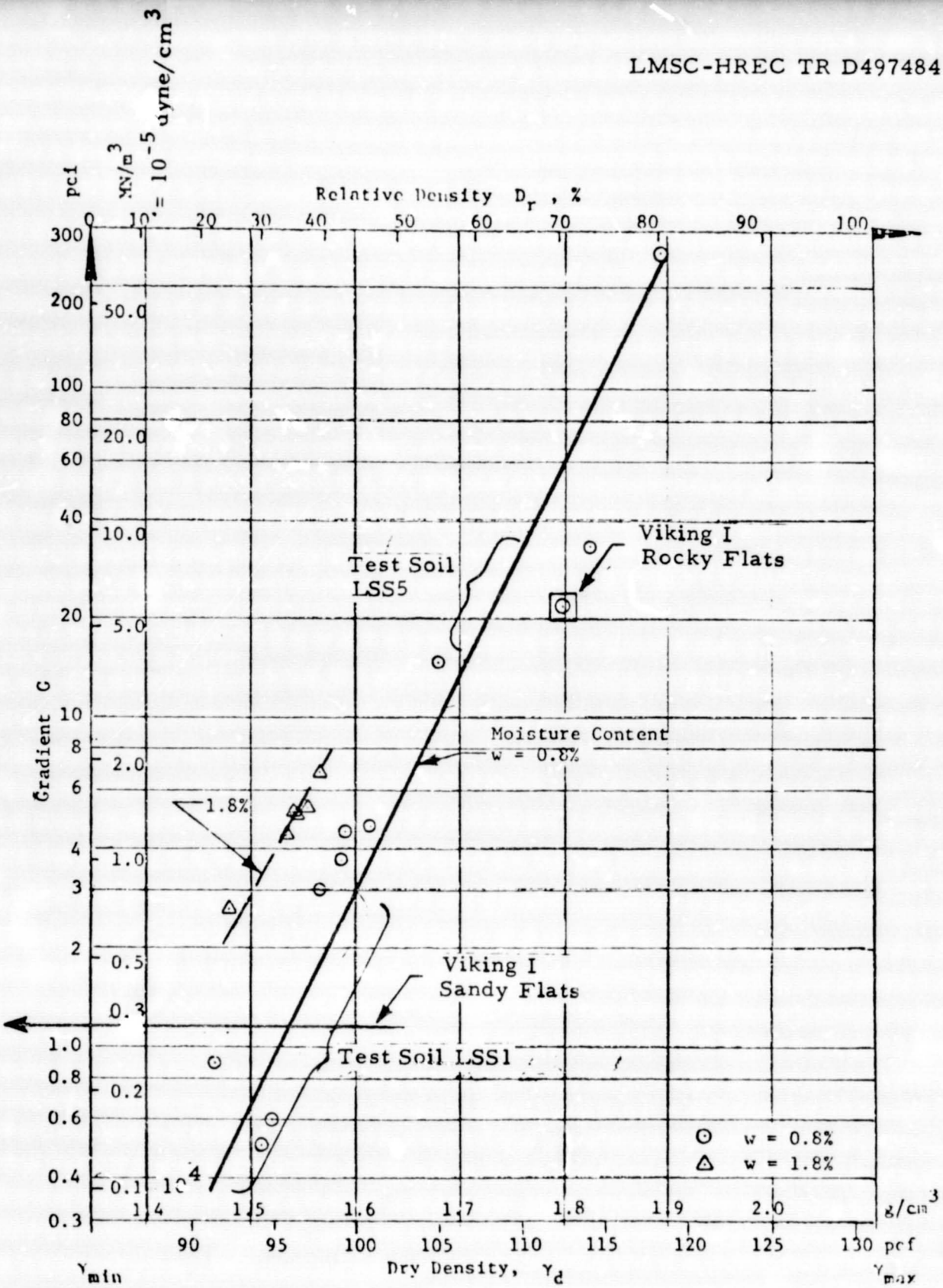

Fig. 2-8 - Relations Among Cone Penetration Resistance Gradient and Density for the Test Soil LSS1 through LSS5 (Ref. 7) Compared with Martian Soil from Viking I Landing Site (Ref. 4)

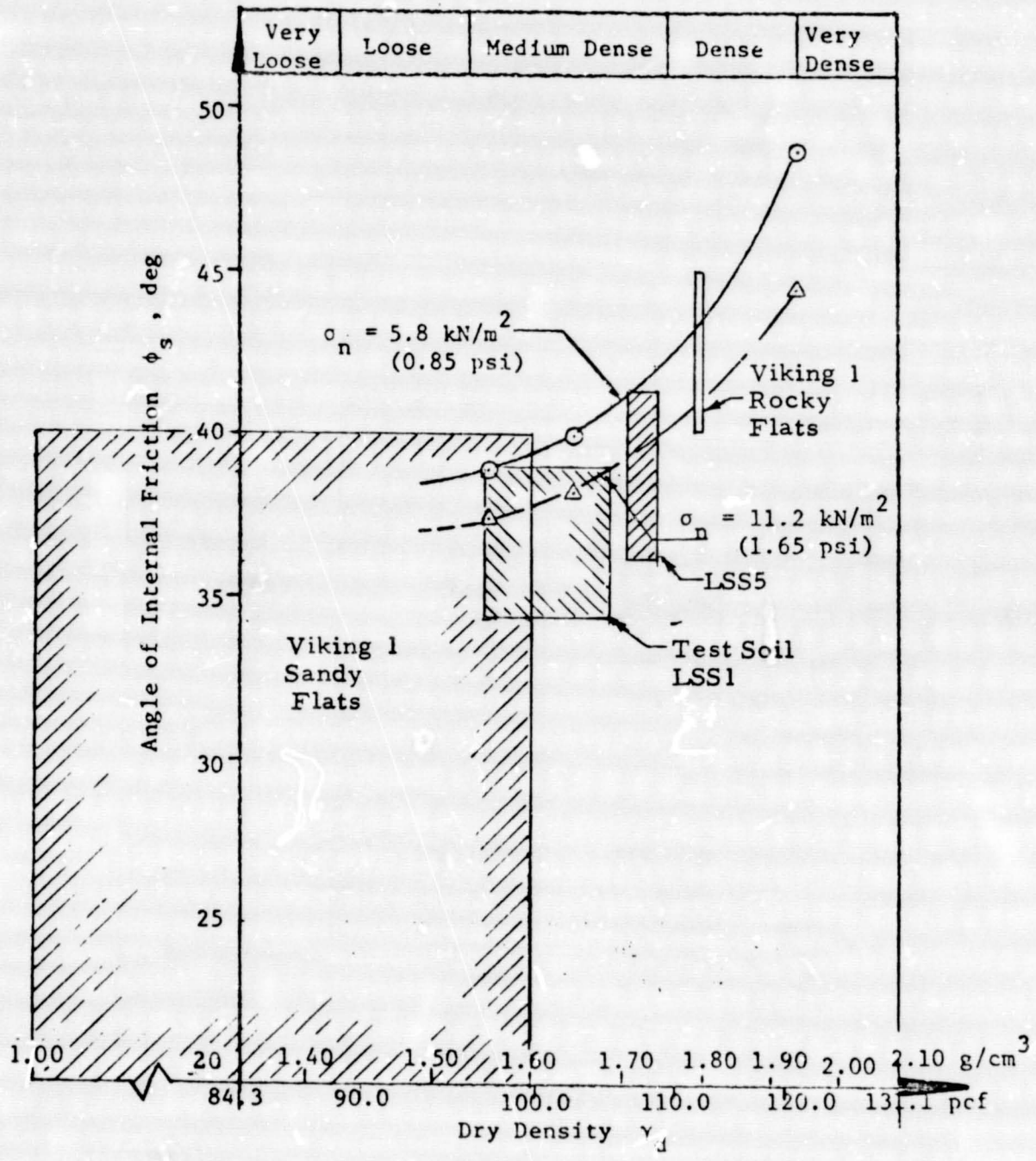

Fig. 2-9 - Relations between Angle of Internal Friction and Density for Test Soil LSS1 through LSS5 (Ref. 7) Compared with Martian Soil from Viking 1 Landing Site (Ref. 4)

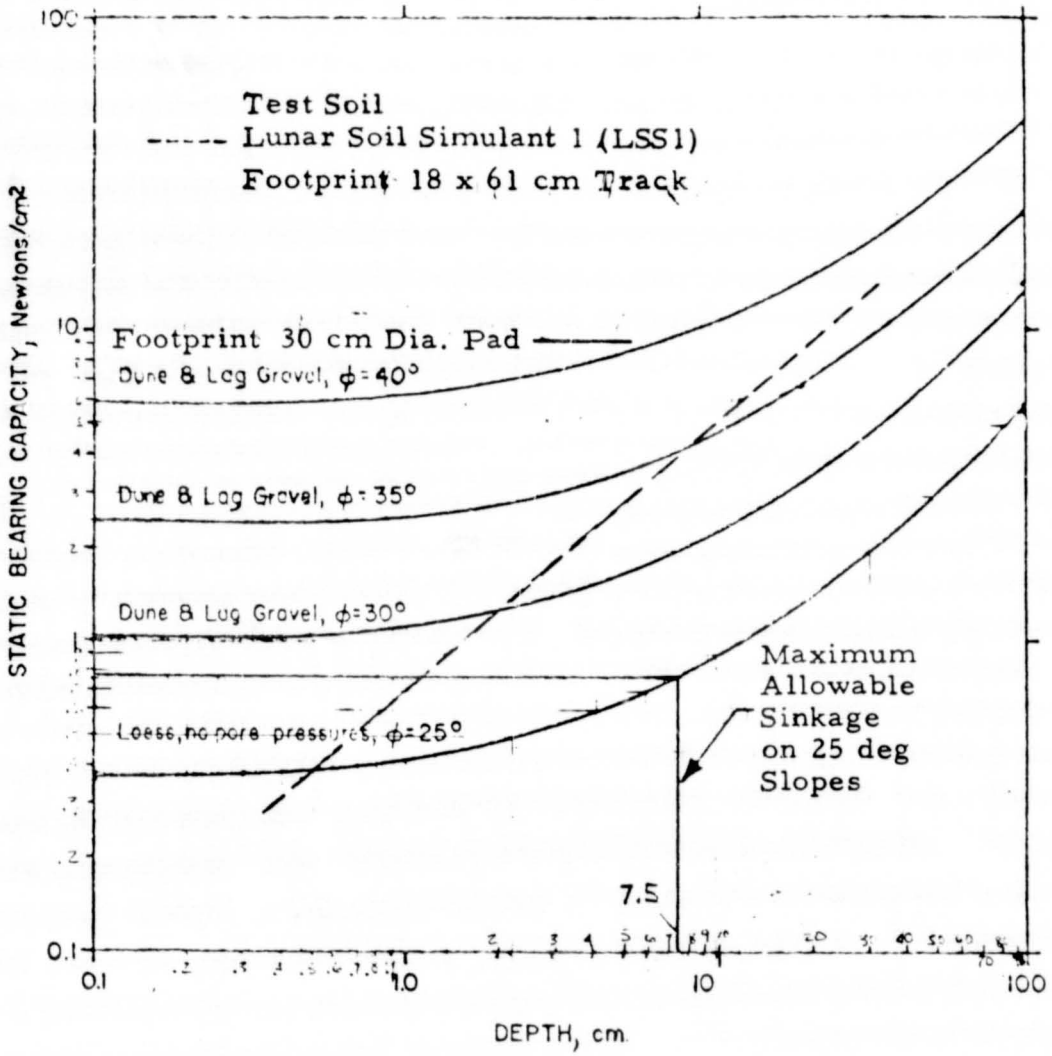

Static bearing capacities computed using Terzaghi's bearing capacity equation for a footpad radius of 15 cm (≈1/2 foot) on a cohesionless Martian soil and the lunar soil. For the Martian dune sand and lag gravels, densities were taken as 1.5 g/cm^3, acceleration of gravity was taken as 375 cm/sec^2, and angles of internal friction used were 30, 35 and 40 degrees. For the loess (lower bound), the density was taken as 1.0 g/cm^3 and the angle of internal friction was taken as 25 degrees.

Fig. 2-10 - Estimated Bearing Strength of Four Soil Models for Mars (Ref. 8) Compared with Test Soil LSS1

As a conservative design approach, footprint requirements have therefore been based on the 1 g/cm^3 loess bearing strength (as plotted in Fig. 2-10) over sinkage. Average sinkage of the LRV wheels during the Apollo 15 moon mission was 1.25 cm. It varied from 0 to 7 cm near fresh craters (Ref. 9). Traction and steering response was considered excellent at low speed and in the relatively smooth lurain traversed where slopes never exceeded 12 deg.

As a conservative design assumption, a maximum allowable sinkage on a 25 deg slope in 1 g/cm^3 density loess of

$$Z_{max} = 7.5 \text{ cm } (3 \text{ in.})$$

was established which calls for a maximum ground contact pressure of

$$P_{max} = 0.78 \text{ N/cm}^2 \text{ (1.12 psi).}$$

Assuming a suspension with roll articulation between front and rear, the nominal pressure in flat terrain is one half the peak pressure as derived in Section 2.1, or

$$P_o = 0.39 \text{ N/cm}^2 \text{ (0.57 psi)}$$

with a nominal sinkage in loess

$$Z_o = 0.5 \text{ cm}$$

according to Fig. 2-10. By comparison the nominal pressure of the LRV wheels was 0.7 N/cm^2 (1 psi).

The severe stowage constraints of the Mobile Viking '79 Lander design led to nominal ground pressures in the range of 0.52 to 0.59 N/cm^2 (0.75 to 0.85 psi, Refs. 10 and 11). The lower ground pressures of the present rover point design should result in superior slope climbing, steering and braking capabilities in soft loess-type soils compared with the LRV and the Mobile Viking Lander.

2.3 LOOPWHEEL MATERIAL PROPERTIES

2.3.1 Loopwheel Core Material

In earlier studies at Lockheed-Huntsville, a wide variety of high strength materials were surveyed for their suitability in manufacturing durable loopwheels of light weight.

A stress and weight analysis resulted in the following material characteristics criterion for loopwheels of maximum strength per unit load and per unit length:

$$\left(\frac{\sigma_F^2}{\rho E}\right) \rightarrow \text{Max.}$$

where

σ_F = flexural fatigue strength at average operating temperature over 5×10^5 load cycles (corresponding to 500 km range)

ρ = density, and

E = Young's Modulus of Elasticity.

While fiber reinforced composites rank highest for terrestrial applications, the low temperature extremes of the Martian night approaching 144 K (-200 F) eliminate composites because of brittleness.

The results of a survey of high-strength metallic alloys for low temperature cyclic load applications is shown in Fig. 2-11.

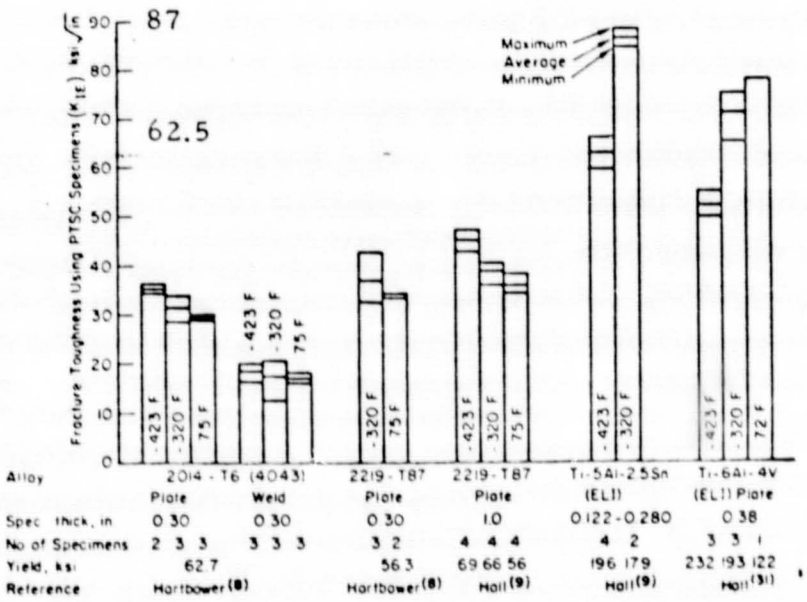

Fig. 2-11 - Effect of Temperature on Fracture Toughness of Aluminum and Titanium Alloys Using Part-Through Surface-Crack Specimens (Ref. 12)

On the basis of fracture toughness using part-through surface-crack specimens (in analogy to a scratch at the loopwheels outer surface) the titanium alloy Ti-5Aℓ-2.5 Sn (ELI-grade) is best suited.

A closer look at the effects of low temperatures on titanium alloys in Fig. 2-12 reveals that substantial embrittlement starts a safe margin below the lowest Martian surface temperatures of 147 K (-195 F).

A conservative number for the flexural fatigue strength of the best suited titanium alloy Ti-5Aℓ-2.5 Sn can be gained from Fig. 2-13. The test temperature (20K) was much lower than the lowest Mars surface temperature. The fatigue strength value for the desired range (70 ksi for 500 K in range) was therefore corrected on the basis of the temperature-fracture toughness relationship plotted in Fig. 2-11. There the Ti-5Aℓ-2.5 Sn (ELI) alloy is shown to improve in toughness as the temperature is raised from -423 to -320 F by

$$\frac{K_I(-320\,F)}{K_I(-423\,F)} = \frac{87}{62.5} = 1.39$$

In the absence of fatigue test data taken at or near the Martian operating temperature range of

$$T_{min} \approx 147\,K\ (-195\,F)$$

$$T_{max} \approx 172\,K\ (-150\,F)$$

it will be assumed that the fatigue strength at the Martian surface temperature is equal to the fatigue strength at 20 K from Fig. 2-13 multiplied by above toughness ratio K_I (-320 F)/K_I (-423 F) from Fig. 2-11 or

$$\sigma_{500\,km,\sigma} = 1.39\,\sigma_{500\,km,\,20K}$$

$$= 671\ MN/m^2\ (97.3\ ksi).$$

This value is considered to be conservative for unnotched material since this alloy exhibits higher toughness as temperature is increased (see Fig. 2-11).

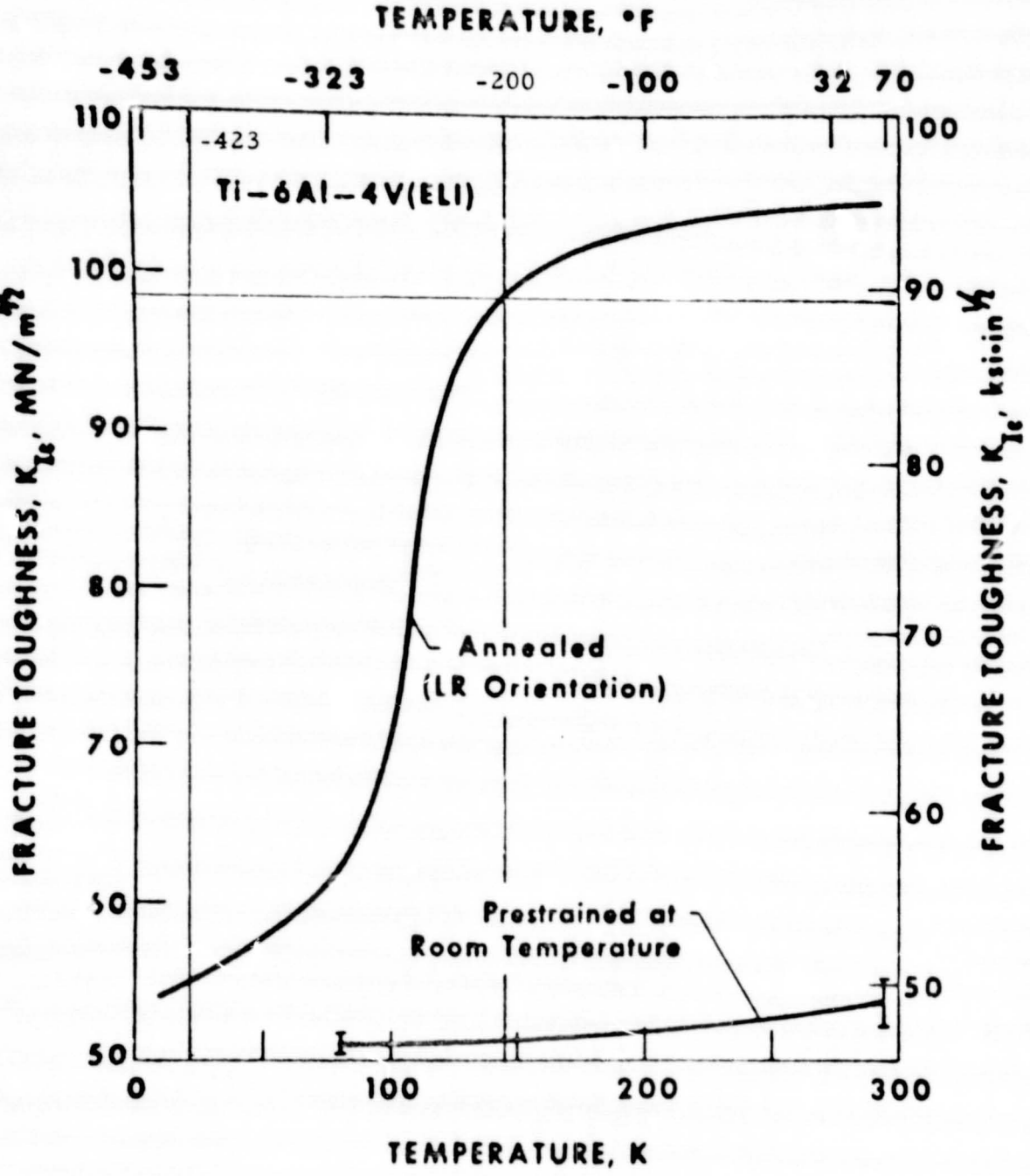

Fig. 2-12 - The Effect of a Room Temperature Prestrain in Biaxial Tension on the Fracture Toughness of the Base Metal (Ref. 13)

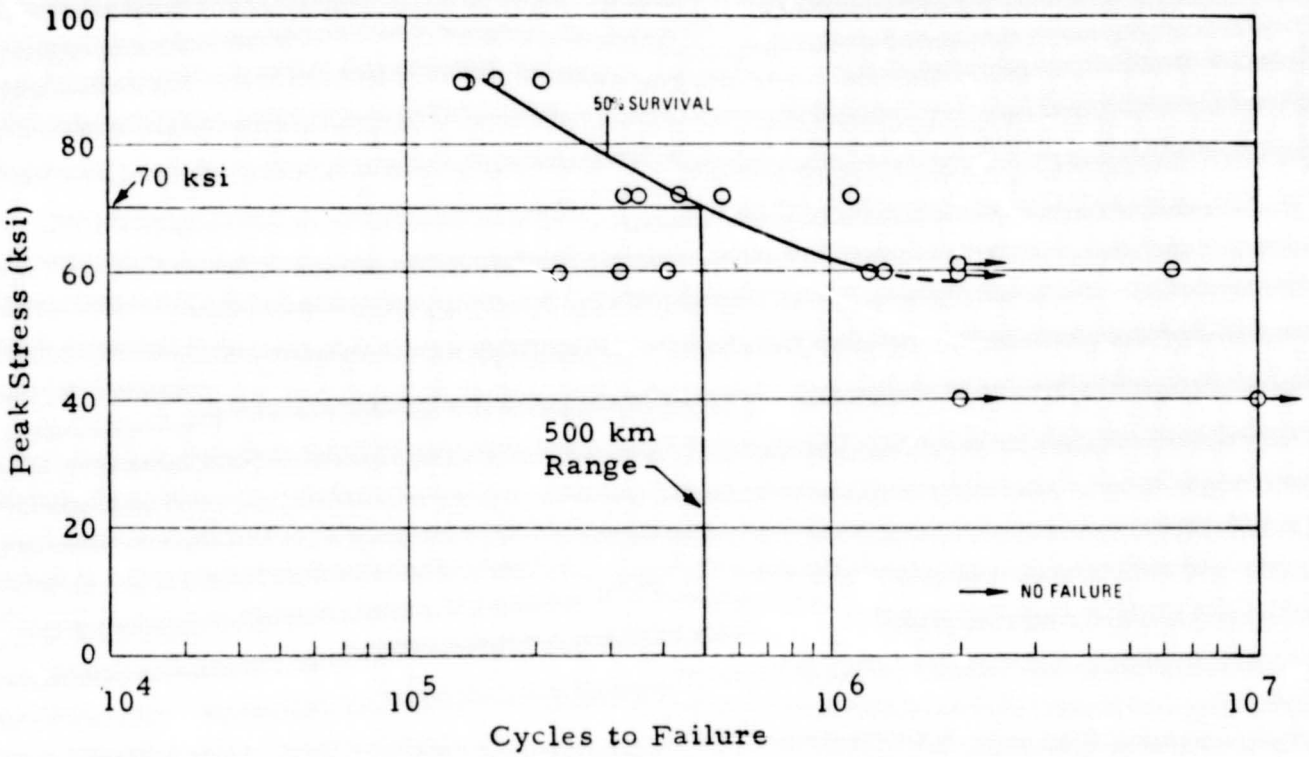

Fig. 2-13 - S-N Curve for Forged Ti-5Al-2.5 Sn Tested at 20K (Ref. 14). Stress Ratio R = -1

Also the stress ratio

$$R = \sigma_{min}/\sigma_{max} = -1$$

used in these fatigue tests was somewhat more severe than the typical stress cycles in the rolling loopwheel which are slightly biased by a tensile preload to

$$R \approx -0.9.$$

A comparison of this alloy's specific loop strength $\sigma_F^2/(\rho E)$ with high-strength steel and aluminum alloys in Table 2 shows that Ti-5Al-2.5 Sn (ELI) is the optimum choice for the load-carrying loopwheel cores.

Table 2

LOOPWHEEL STRENGTH
Per Unit Load, Per Unit Length

Material	σ_F^* MN/m^2	Test Temp.	Density, ρ g/cm^3	E GN/m^2	Spec. Strength $\sigma_F^2/(\rho E)$
Ti-5Al-2.5 Sn (ELI) Annealed	483**	20K	4.48	107	0.487×10^6
Steel 300 M	690	293K (RT)	7.83	200	0.304×10^6
Al 2014-T6	193	77K	2.80	72.4	0.184×10^6

*Flexural fatigue strength at 5×10^5 cycles (500 km) at temperature listed.

**Forged; grain size of spin formed loopwheels should be similar to forged test specimens

2.3.2 Loopwheel Tread Material

A tread on the outer loopwheel surface must perform two functions: (1) improve traction by well spaced, deep grouser patterns; (2) protect the load-carrying titanium core from surface scratches and abrasion.

The tread material should be of low density to minimize weight and of high wear resistance and elasticity at 144 K temperature. Furthermore it must withstand the sterilization heat treatment (112 C $\pm$ 2C) without excessive set or softening.

Of all the engineering plastics screened, only ultrahigh molecular weight (UHMW) polymer, a high density polyethylene in the molecular weight range between 2×10^6 to 6×10^6 satisfies all of the above requirements. It's major physical properties are

Density	0.94 g/cm^3
Vicat softening point	136 C
Brittle point	< 100 K
Modulus of elasticity at room temperature	517 MN/m^2
Impact strength (I_{Zod} Notched, ASTM 255-65)	11.6 Nm/cm^2.

Tensile strength at room temperature and at 120 C (8 C above sterilization temperature) is plotted in Figs. 2-14 and 2-15. Although the lowest test temperature of -110 C is 16 C above the expected Martian temperature low, extrapolations of ultimate and yield stress to -126 C provide good estimates for preliminary design purposes.

Flexural fatigue data are shown in Fig. 2-16. In the "non-isothermal" tests the specimens softened due to heating as a result of the fast cycle rate of 20 Hz. The temperatures of the uncooled specimens are also listed. In the "isothermal" test procedure the specimen was kept at room temperature by cooling. In the absence of low temperature fatigue test data, a

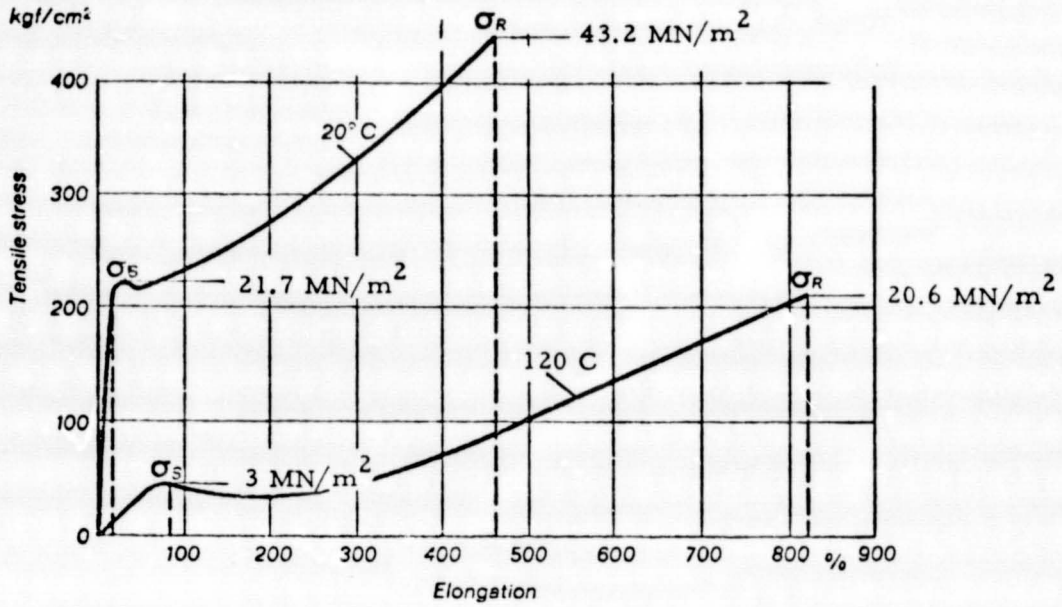

Fig. 2-14 - Stress-Strain Diagram of Candidate Tread Material UHMW Polymer at Room Temperature and 120 C (Ref. 15)

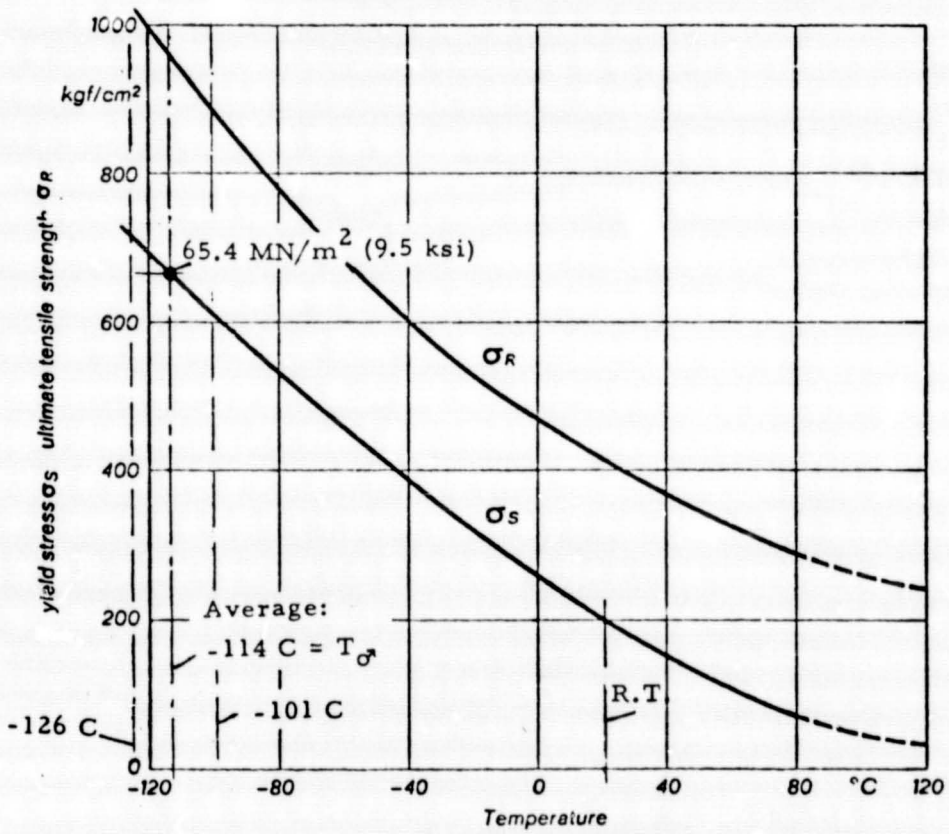

Fig. 2-15 - Tensile Strength of UHMW Polymer as a Function of Temperature (Ref. 15)

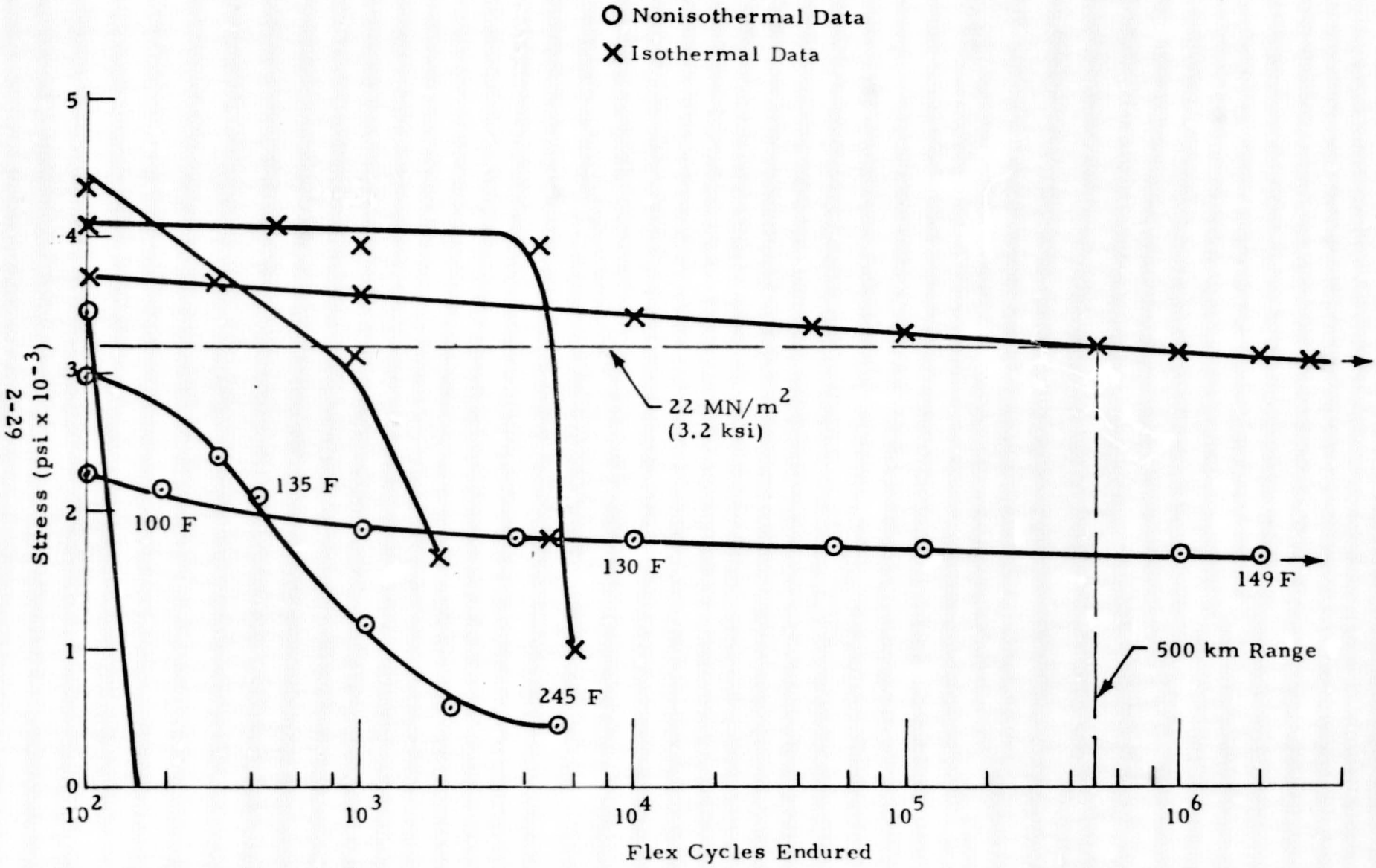

Fig. 2-16 - Flexural Fatigue S-N Curve for UHMW Polymer at Elevated and Room Temperature (Ref. 16)

conservative assumption would be to consider fatigue strength constant from room temperature to -126 C.

A comparison of this polymer's excellent abrasion resistance with other commonly used wear surface materials is given in Table 3.

Table 3

MATERIAL RESISTANCE TEST RESULTS

ABRASIVE RESISTANCE

SAND SLURRY TEST

Each material listed below was rotated 7½ hours @ 1750 r.p.m.
Carbon Steel = abrasive rating of 100
The weight loss for each material is relative to 100
The lower the figure, the better the abrasive resistance.

UHMW POLYMER	17	TFE/glass fiber	113
Nylon	31	Normal MW polyethylene	125
High MW polyethylene	44	Phosphor bronze	193
TFE	72	Yellow brass	409
Stainless Steel	84	Phenolic laminate	571
Polypropylene	87	Hickory wood	967
Polycarbonate	96	Hi Carbon Steel	100
Polyacetal	110		

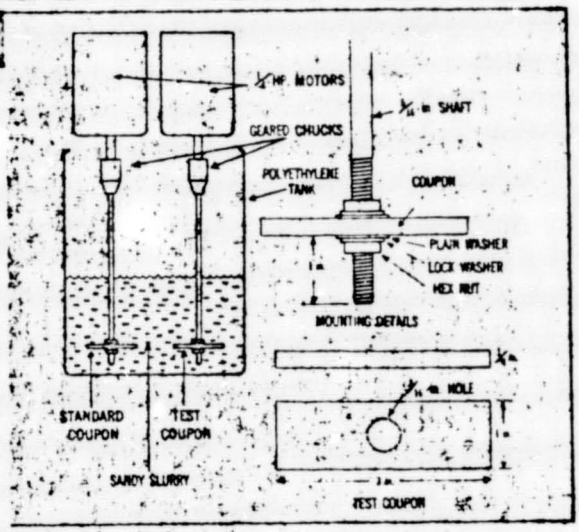

Source: Hercules, Inc.

The only shortcoming of the material is a low coefficient of friction (similar to Teflon) which, according to the manufacturer, may be increased by adding suitable fillers. By a careful tread design, there should be no adverse effects on tractive capabilities.

2.4 COMPARISON OF STEERING CONCEPTS

Four steering concepts were evaluated for their mission suitability, complexity, impact on vehicle design and failure characteristics. They were:

- Scuff steering
- Wagon steering
- Ackermann steering, and
- Dual-Ackermann steering.

Some of the most important properties for a comparative evaluation were found to be very difficult to determine within the scope of this study. They were power requirements, wear characteristics, steerability in soft soil and between rocks and the probability of encountering hazards during a steering maneuver. All known approaches to model the interactions between a track or loopwheel and the soil during steering require detailed information about tread configuration, pressure distribution, c. m. location and soil properties, all of which are not well defined at this time. However, the total area compacted by the four loopwheels during typical steering maneuvers was found to be a direct measure of parasitic drive energy, wear, steering responsiveness and of the probability of encountering hazards during the maneuver.

To provide maximum comparability between the four steering concepts, the steering maneuver was selected so that at the start and end the rover would be at identical locations independent of the type of steering. The four test maneuvers are illustrated in Fig. 2-17. A 30 deg change in direction of travel is assumed. For the wagon-steered and Ackermann-steered concept the effective steering deflection of the front wheels was also assumed to be 30 deg throughout the turn until the heading change is completed. The resulting average turn radius from the rover's center of mass was in the order of one overall rover length with the exception of scuff steering where the turn radius was zero and the rover then followed a straight course to the common terminal location.

The results of this comparison are plotted in Fig. 2-18. The bar chart shows total compacted area as well as that fraction of total area swept by side slipping which is higher in energy consumption and in risk of debris ingestion.

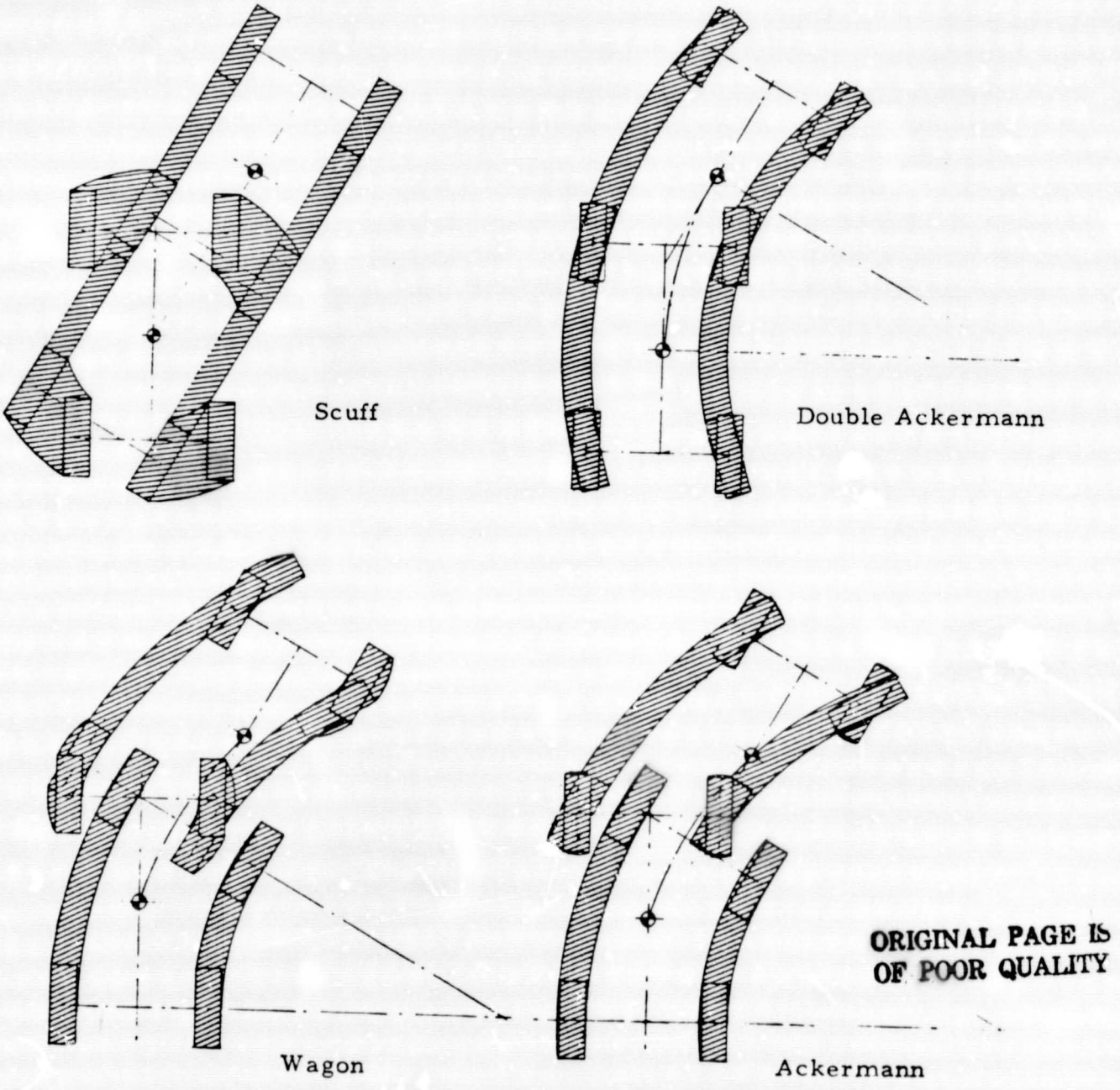

Fig. 2-17 - Comparison of Total Area Compacted During 30-deg Turn Maneuver

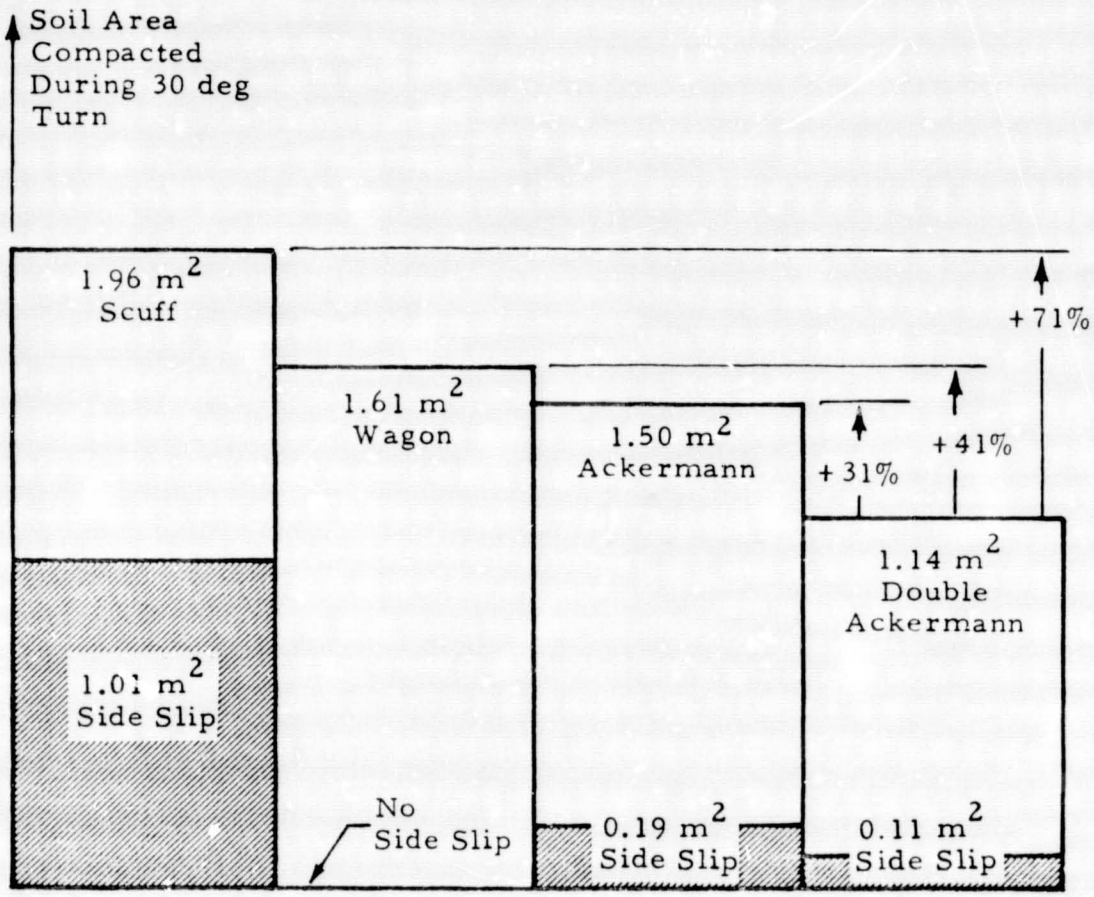

Fig. 2-18 - Comparison of Compacted Soil Area During Turn as a Direct Measure of Energy Consumption, Wear of Loopwheels and Probability of Hazard Encounters

The price paid for the simplicity of scuff steering is readily apparent. It is the least energy efficient, most abrasive and most hazardous concept as far as debris ingestion during side slipping and probability of rock encounters is concerned. Over half of the total compacted area is swept during the initial side slipping.

Wagon and Ackermann steering are about equal in energy consumption, wear and probability of terrain hazard encounters. The absence of any pure side slipping during Wagon steering conpensates for its slightly larger total compacted area in all three performance categories.

Double Ackermann steering turns out to be tne optimum concept as far as energy efficiency, loopwheel wear and probability of hazard encounters is concerned. Throughout the turn the rear loopwheels follow the rut of the front loopwheels thereby improving traction and reducing the hazards associated with covering new ground.

Good insight into the improved mobility when following an existing rut can be gained from inspecting data from loopwheel tests performed in Lunar Soil Simulant (LSS) at the U.S. Army Engineer Waterways Experiment Station and reported in Ref. 7.

Typical test data from first and second passes of a single loopwheel test unit in the same path of a soil bin are repeated in Table 4. Additional evaluation criteria related to impact on vehicle design, stowage/deployment, complexity and cost of hardware and control software, and single point failure tolerance were used to compare the four concepts. The results are compiled in the evaluation matrix, Table 5.

Relative scores in each of nine categories were totaled with and without weighting factors. The (admittedly subjective) weighting factors were selected with respect to the impact on probability of mission success. Design related criteria were therefore weighted lower than those which affect functional aspects.

Table 4

FIRST AND SECOND PASS LOOPWHEEL TEST
DATA FROM REF. 7 SHOW SUBSTANTIAL MOBILITY
IMPROVEMENT FOR REAR LOOPS FOLLOWING FRONT LOOPS' RUT

Test No.	Pass No.	Traction* (P/W')	Specific Energy** (PN')	Efficiency+ (η)
A72-012-6	1	0.22	0.47	0.47
	2	0.54	0.71	0.76
A72-014-6	1	0.51	0.72	0.72
	2	0.62	0.80	0.78
A72-017-6	1	0.37	0.58	0.63
	2	0.43	0.55	0.79

*P = pull developed in direction of travel

W' = actual loopwheel load component normal to surface; on a slope α: $W' = W\cos\alpha$

**PN' = power number = $M\omega/(W' V)$, where
M = actual torque at gear head/sprocket connection,
ω = sprocket speed
V = actual rover speed.
Thus, PN' = energy consumed per unit load per unit distance traveled or power (watt) per N load per m/sec speed.

+Efficiency $\eta = \frac{P/W'}{PN'} = \frac{PV}{M\omega}$ = propulsive output power PV/mechanical input power at drive sprocket.

Table 5

EVALUATION AND SCORING MATRIX TO SELECT OPTIMUM STEERING CONCEPT

Evaluation Criterion	Weighting Factor Aimed at Maximum Probability of Mission Success	Score* Scuff		Wagon		Ackermann		Double Ackermann		Remarks
			Weighted		Weighted		Weighted		Weighted	
Energy Efficiency	2	0	0	3	6	3	6	5	10	Based on Soil Area Compacted During Turn
Tread and Drive Train Wear	3	0	0	4	12	3	9	5	15	
Probability of Hazard Encounters†	3	0	0	3	9	3	9	5	15	
Minimum Turn Radius	3	5	15	3	9	3	9	4	12	
Impact on Vehicle Design	1	5	5	2	2	3	3	2	2	
Impact on Stowage and Deployment	1	5	5	2	2	3	3	2	2	
Hardware Complexity	2	5	10	4	8	3	6	2	4	
Control Software Complexity	1	5	5	3	3	2	2	0	0	
Failure Tolerance										
a. One Loopwheel Drive Out	3	0	0	4	12	4	12	5	15	
b. One Steering Activator Out	3	5 (N/A)	15	3 (Lock & Go to Scuff)	9	3 (Use Scuff or Tie Rod Between Left and Right Loopwheel)	9	4 (Use Std. Ackermann Steering)	12	
Total Score Weighted		30	55	31	70	30	68	34	87	

*Relative Scoring: 5 = Best, 0 = Unsatisfactory

†Includes probability of debris ingestion during turn.

Proposed Baseline Steering Concept

In both scores – with and without weighting factors – double Ackermann steering ranked highest, followed by Wagon steering with Ackermann steering a close third or tied for second place.

The simplicity of a scuff steer rover compensates for it' s operational weaknesses in the plain scoring to keep the score in the second place region. However, the mission success oriented score falls off markedly to a clear lowest rank. However, scuff steering can serve as a backup mode for any of the other three concepts in case of steering actuator failure(s).

On the basis of this evaluation double Ackermann steering is proposed as the baseline steering concept with single Ackermann steering as primary backup mode in case of front or rear steering actuator failure and scuff steering as secondary backup mode in case of front and rear steering actuator failures.

2.5 TRADE STUDIES AND SELECTION OF POINT DESIGN

After worst case soil conditions, maximum allowable ground contact pressure and worst case loads were established, trade studies were required to determine the optimum loopwheel dimensions and loopwheel mass. As a valuable and efficient tool in these trade studies design charts were prepared and arranged so that all major parameters can be determined graphically. The design charts of Fig. 2-19 not only provided a baseline loopwheel configuration for the present assumptions on soil conditions, allowable sinkage and worst case loop loads (which is shown in Fig. 2-19), but they also can be used to quickly assess the impact of possible changes in load or soil conditions or in loopwheel dimensions. In the following section, the intended use of the design charts will be illustrated by the example of the current rover point design.

In Sections 2.1 and 2.2, the following maximum load and allowable ground contact pressure data were established:

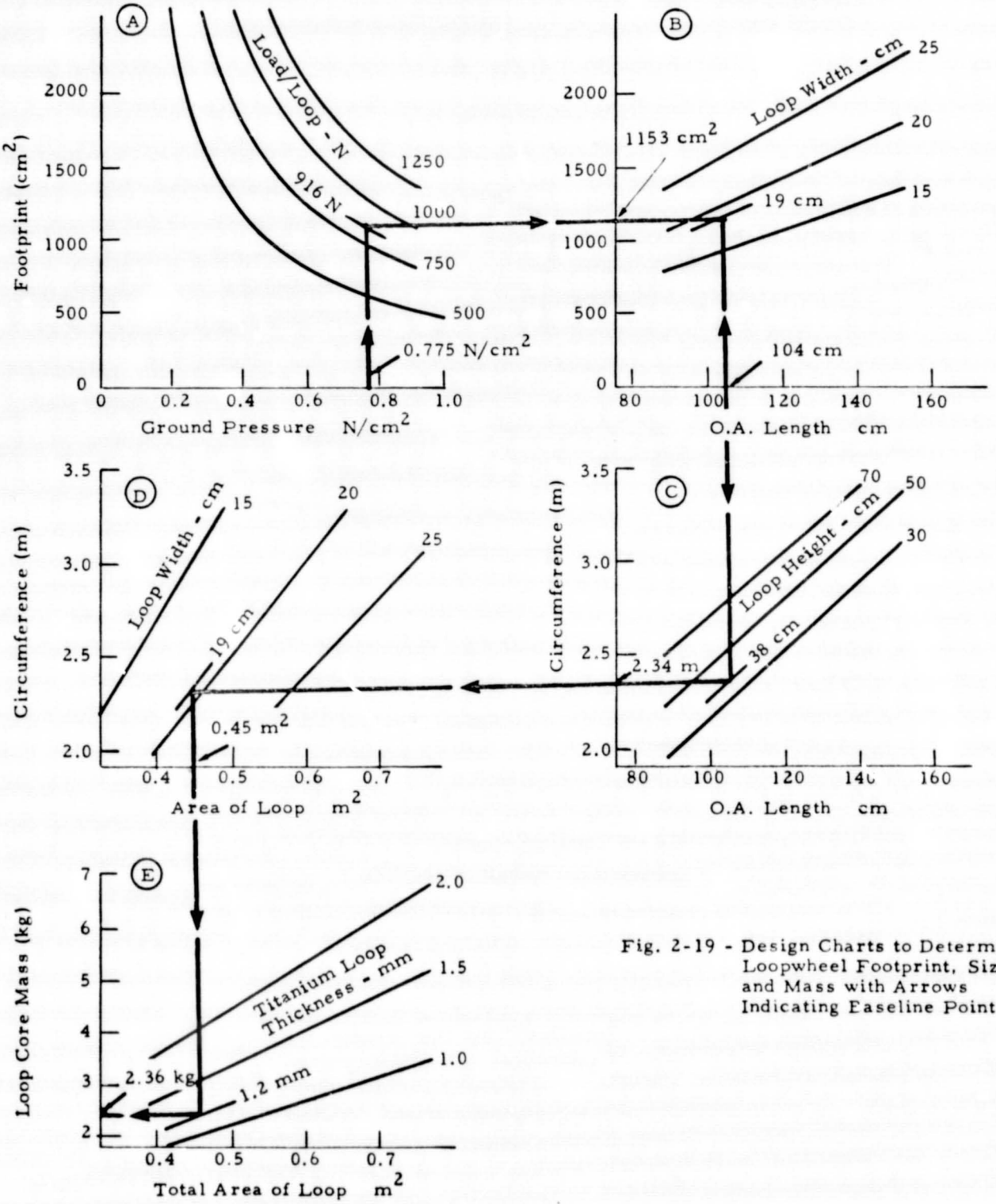

Fig. 2-19 - Design Charts to Determine Loopwheel Footprint, Size and Mass with Arrows Indicating Baseline Point

- Maximum load per loop: 916 N, assuming suspension Option II with roll articulation between front and rear end;
- Maximum ground contact pressure (on 25 deg slope): 0.775 N/cm^2
- Stowage and deployment constraints as shown in the JPL point design (Ref. 3) were assumed to dictate a maximum overall loopwheel length of 104 cm.

As the first step in sizing the loopwheel, the ground pressure was entered into design chart (A). It intersects the 916N max. load per loop curve in (A) at an ordinate

$$A_{footprint} = 1153\ cm^2.$$

Cross plotting this ordinate into Chart (B) and entering the specified maximum overall loop length in the abscissa of (B) defines the loopwheel width (at the tread) in Chart (B). Cross plotting the overall length into Chart (C) and selecting a loop height consistent with stress considerations

$$H_{Loop} = 0.365\ L_{Loop}$$

$$= 0.365 \cdot 104 = 38\ cm$$

defines an intersect point in Chart (C) whose ordinate is loop circumference

$$C = 2.34\ m.$$

Cross plotting this ordinate into Chart (D) defines a point on the 19 cm loop width curve whose abscissa represents the total area of the loop core material. The intersection of the cross plotted abscissa with the straight line in Chart (E) which represents the selected thickness of the titanium core (found by load/stress/deflection analysis described in the next section) defines the mass per loop core. In the present point design, the loop core area from Chart (D) is

$$A_{core} = 0.45\ m^2.$$

A loop thickness

$$t = 1.2\ mm$$

then leads to a mass per loop core

$$m_{core} = 2.36 \text{ kg} .$$

Several other loopwheel configurations were investigated before the present baseline design was selected.

As footprint requirements and/or stowage constraints and worst case loads become better defined, these charts should be efficient aids in assessing the impact of changes on loopwheel dimensions and mass.

2.6 STRUCTURAL ANALYSIS AND WEIGHT ESTIMATION

2.6.1 Loop Core Analysis

A finite element computer code was developed by Lockheed-Huntsville as an efficient tool in loopwheel analysis and design. It is based on the Nonlinear Elastic-Plastic Structural Analysis Program (NEPSAP) and represents the loopwheel' s load carrying core by 480 curved plate elements.

After the major loopwheel loads and dimensions for the present point design and the most promising material (Ti-5Aℓ-2.5 Sn) had been established, the loop' s transverse curvature and material thickness were determined by a parametric NEPSAP analysis.

Portions of a typical output plot are shown in Fig. 2-20, illustrating the unloaded and partially loaded loopwheel. The ground contact pressure is assumed to be distributed in a cosine law along the longitudinal direction.

The objective of the parametric study was to obtain well distributed loads over the entire footprint and the desired loop height of 38 cm or less at allowable stress levels which provided sufficient margins to account for stress concentrations due to surface scratches.

At the same time sufficient sprocket-to-loopwheel engagement pressure has to be maintained to assure positive engagement under maximum side loads.

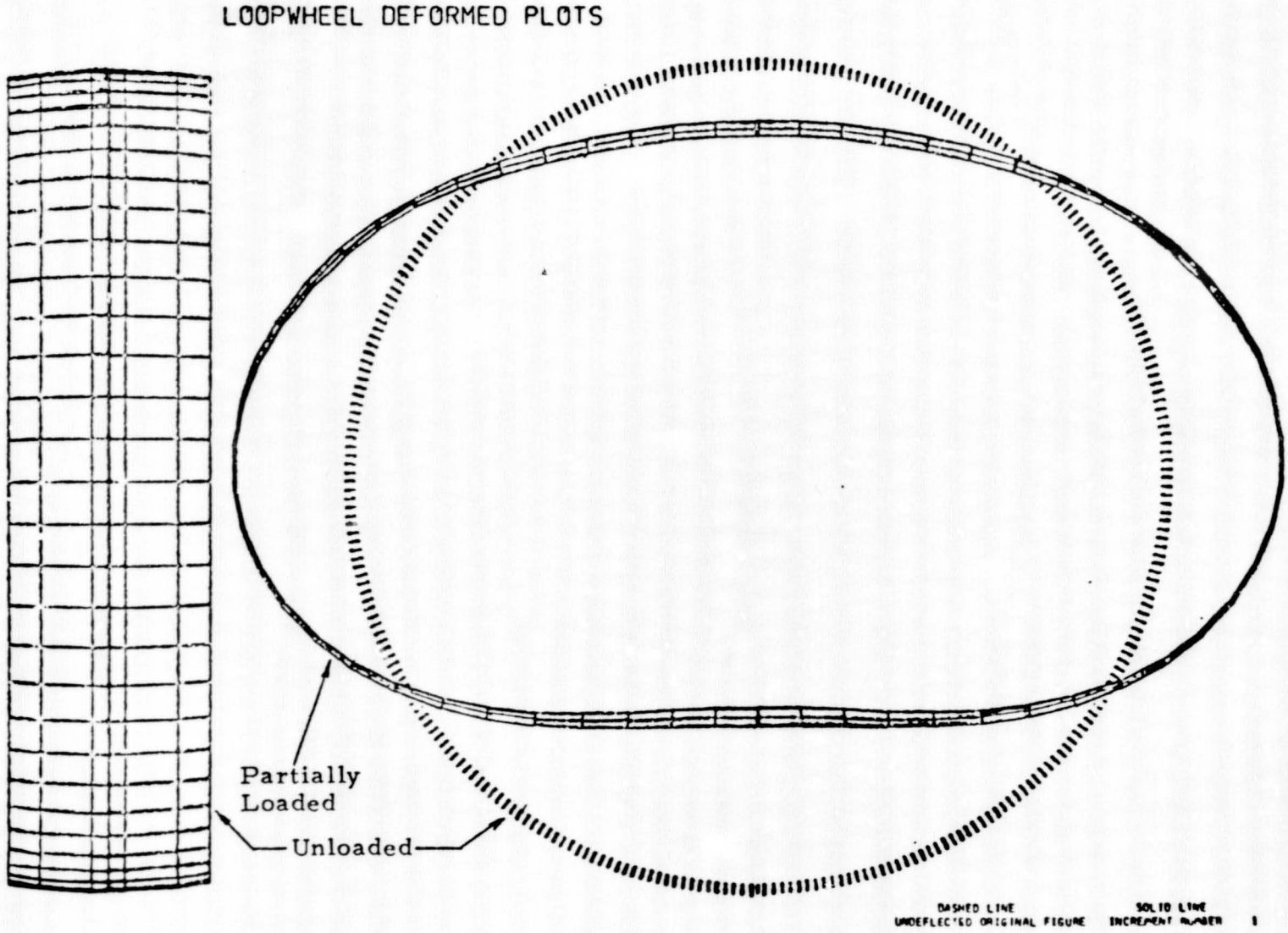

Fig. 2-20 - Typical Output Plots of Lockheed's Structural Analysis Program for Loopwheels

Following a separate analysis, the swing arm/sprocket/load roller configuration was designed which provides the required sprocket engagement pressure at the specified normal load. To this end the moment arm a and vertical height b to the swing arm pivot axis (Fig. 2-21) was systematically varied until sufficient engagement pressure was assured by analysis. The additional loop load caused by Lockheed's pivoted sprocket suspension was included in the subsequent structural NEPSAP analysis.

The following loop core dimensions were found to satisfy the requirements of the present point design:

Loop Shape Under 458 N Load:

OA Height:	38 cm
OA Length:	104 cm
Core Thickness:	1.2 mm
Width of Load Carrying Core:	19 cm
Transverse Curvature (unloaded):	R = 56 cm
Circumference	2.34 m
Maximum Cyclic Tensile Stress:	127.8 MN/m^2 (18.5 ksi)
Maximum Cyclic Compressive Stress:	115.8 MN/m^2 (16.8 ksi)
Loop Core Mass:	2.36 kg.

Major loopwheel core dimensions and the details for a roller chain-type sprocket engagement along both edges are shown in the preliminary design drawing, Fig. 2-22. In the design shown, the roller mounts would be formed from the flat seamless titanium ring of uniform thickness by bending in a die. An alternate manufacturing method is under study: the loopwheels would be spinformed with thick edge sections of approximately 6.5 mm wall (0.255 in.) and the desired 1.2 mm wall between edge sections. The roller mounts would be machined. This second approach appears to have less risk of stress concentrations from fabrication and promises to lead to better dimensional stability.

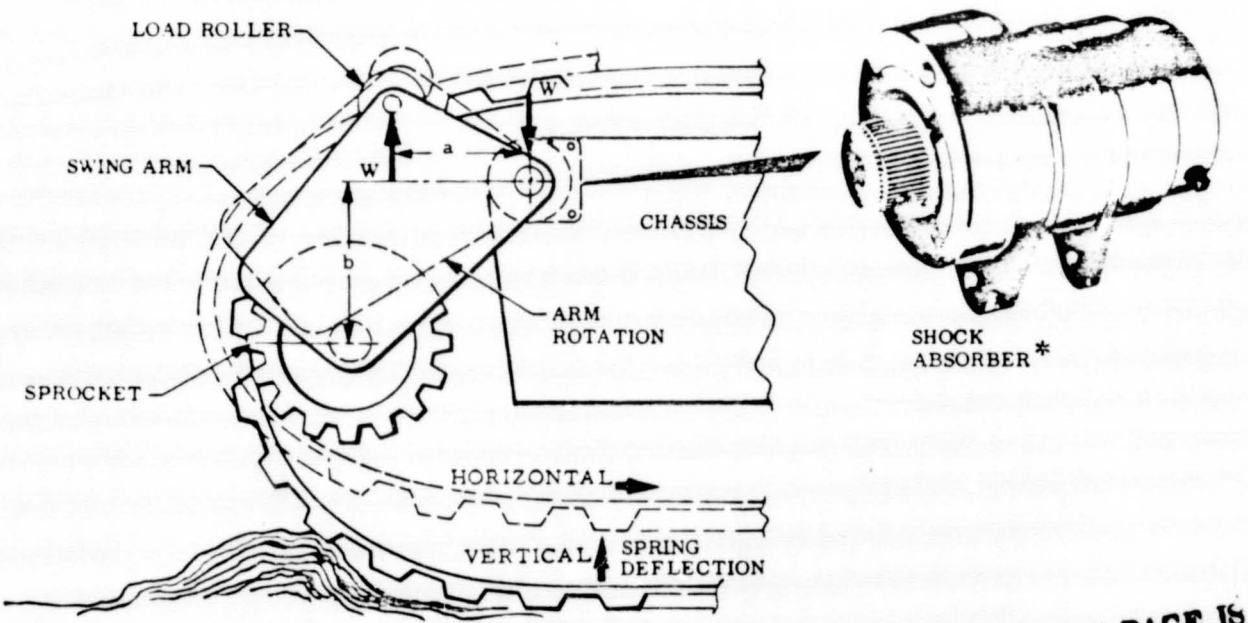

*Optional

Fig. 2-21 - Loopwheel Suspension and Damping Concept: Vehicle weight, W, is transmitted to loop by upper load roller. Moment (W · a) keeps drive drum in contact with loop. Spring deflection results in arm and damper rotation α to dissipate energy. Depending upon direction of terrain disturbance, loopwheel deflects vertically or horizontally or in both directions.

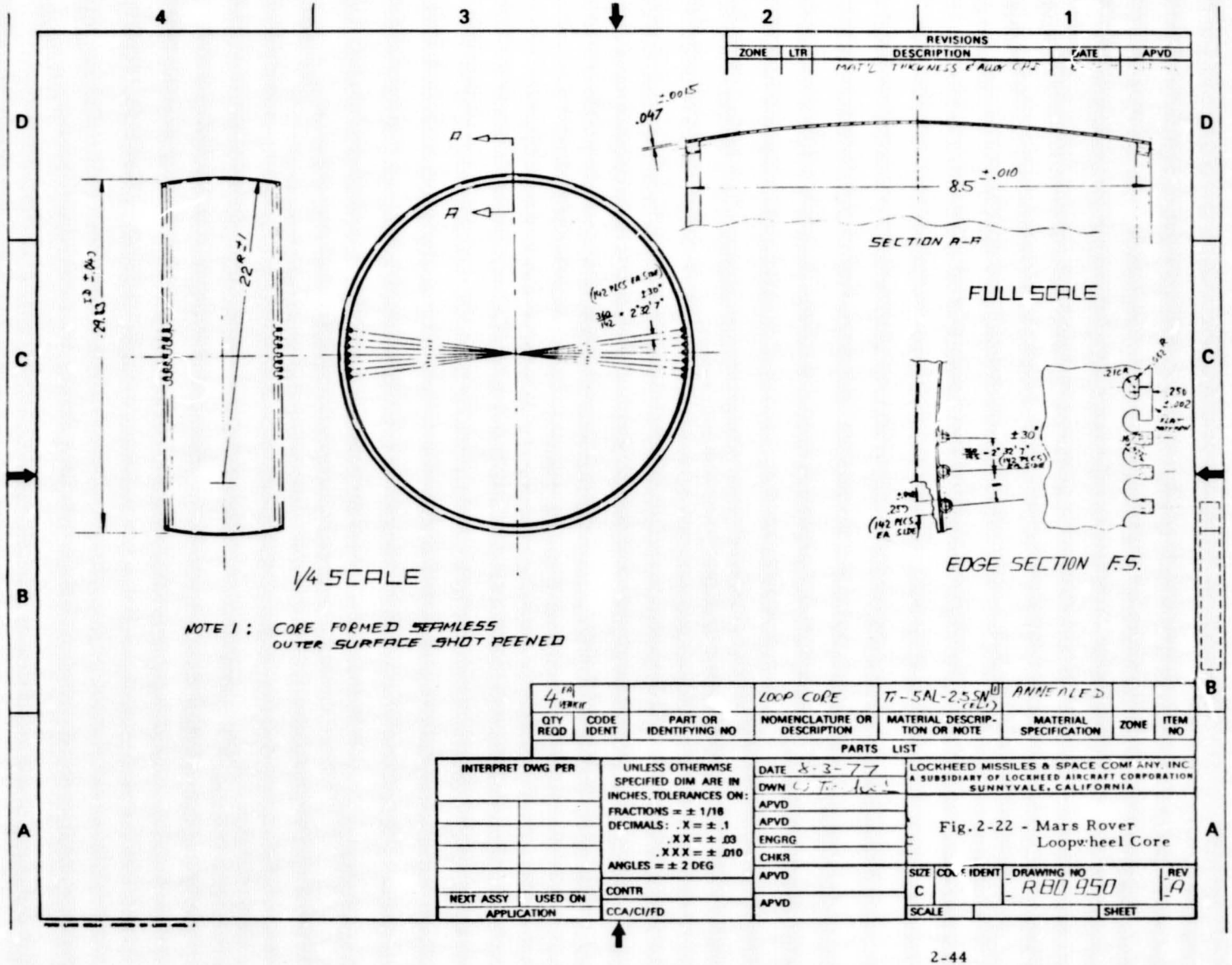
REVISIONS
ZONE | LTR | DESCRIPTION | DATE | APVD
SECTION A-A
FULL SCALE
1/4 SCALE
EDGE SECTION F.S.
NOTE 1: CORE FORMED SEAMLESS
OUTER SURFACE SHOT PEENED
4 REQD | LOOP CORE | Ti-5AL-2.5SN (ELI) | ANNEALED
QTY REQD | CODE IDENT | PART OR IDENTIFYING NO | NOMENCLATURE OR DESCRIPTION | MATERIAL DESCRIPTION OR NOTE | MATERIAL SPECIFICATION | ZONE | ITEM NO
PARTS LIST
INTERPRET DWG PER
UNLESS OTHERWISE SPECIFIED DIM ARE IN INCHES. TOLERANCES ON:
FRACTIONS = ± 1/16
DECIMALS: .X = ± .1
.XX = ± .03
.XXX = ± .010
ANGLES = ± 2 DEG
NEXT ASSY | USED ON
APPLICATION
CONTR
CCA/CI/FD
DATE 3-3-77
DWN
APVD
APVD
ENGRG
CHKR
APVD
APVD
LOCKHEED MISSILES & SPACE COMPANY, INC.
A SUBSIDIARY OF LOCKHEED AIRCRAFT CORPORATION
SUNNYVALE, CALIFORNIA
Fig. 2-22 - Mars Rover Loopwheel Core
SIZE C | CODE IDENT | DRAWING NO RBD 950 | REV A
SCALE | SHEET

2.6.2 Loopwheel Tread Analysis

In close coordination with potential suppliers of the candidate tread material, UHMW polymer, the following manufacturing approach was identified as most promising: The tread material will be bonded to the outer surface of the seamless titanium loop core by compression molding in place. The tread material will be reinforced in tear strength by one or more plies of fabric close to the titanium core (Fig. 2-23). For maximum adhesion the tread material would also fill the D-shaped cutouts along the edges of the core and be wrapped around the inside core surface in strips of approximately 20 mm width (0.79 in.).

The most cost effective manufacturing approach appears to be molding the tread material in uniform thickness and form the desired grousered tread by subsequent machining. Chevron-style grousers would be separated by sections of minimum height for maximum traction as shown in Fig. 2-24. The minimum thickness between grousers must be selected with the following conflicting objectives:

- Provide maximum protection to the highly stressed loop core from rock damage and soil abrasion. (Thick tread is safest!)
- Keep cyclic stress levels in tread low to satisfy fatigue life requirements of 500 km without fatigue cracks. (Thin tread is safest!)
- Minimize thermal stresses in tension caused by different linear coefficients of thermal expansion, namely

$$\epsilon_{\text{polymer}} = 61 \times 10^{-6}/\text{K}$$

$$\epsilon_{\text{Ti-5Al-2.5 Sn}} = 5.2 \times 10^{-6}/\text{K}.$$

In operation the tread is subjected to cyclic bending cycles of the following nominal peak strain ϵ_B with respect to the unloaded cylindrical configuration (a) in Fig. 2-25:

$$\epsilon_B = \left(\frac{t}{2} + t_p\right)\left(\frac{1}{R} - \frac{1}{R_o}\right) \quad ,$$

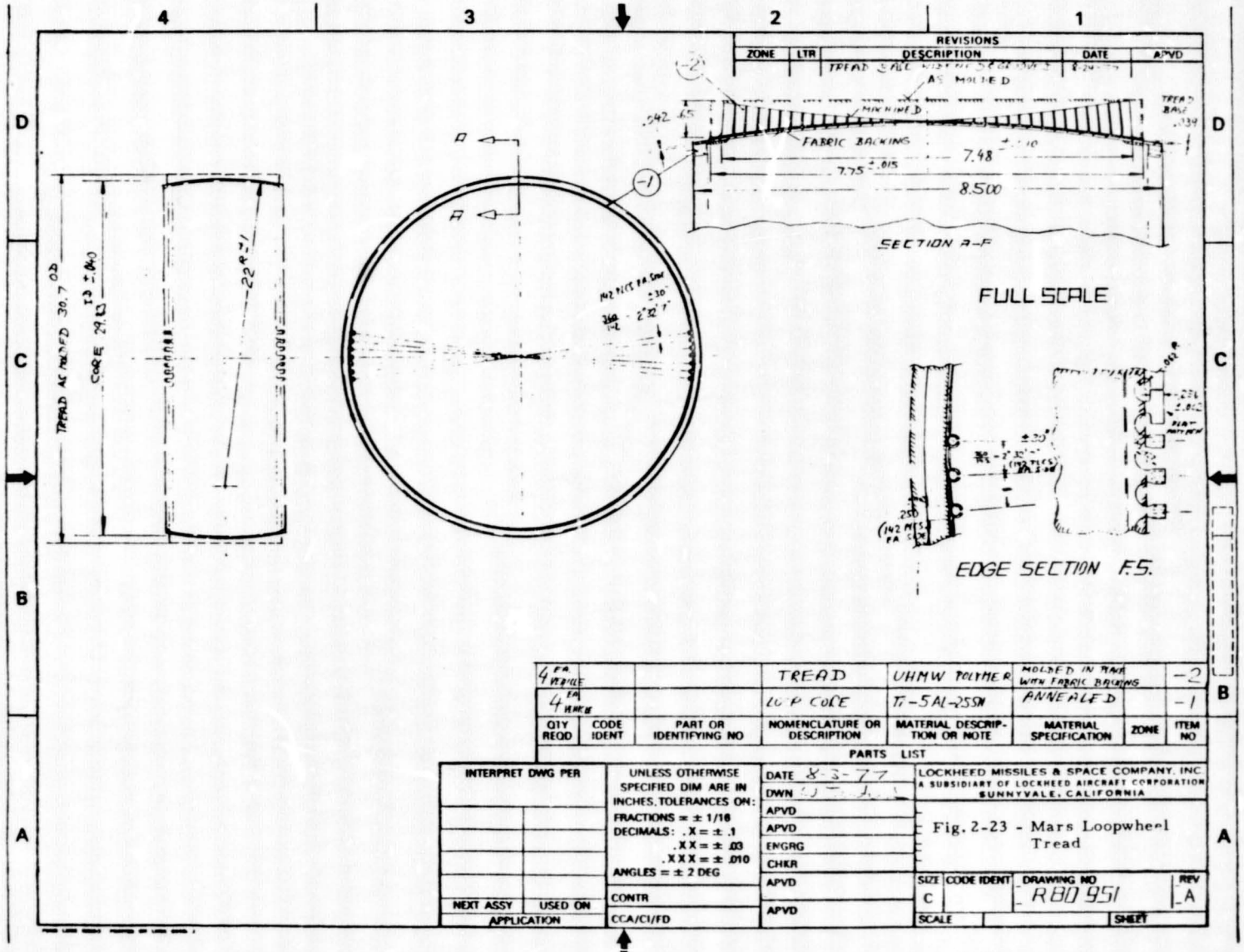
REVISIONS
ZONE | LTR | DESCRIPTION | DATE | APVD
AS MOLDED
MACHINED
FABRIC BACKING
7.48
7.75 ±.015
8.500
SECTION A-F
FULL SCALE
EDGE SECTION F.S.
TREAD AS MOLDED 30.7 OD
CORE 29.62 ±.040
22.5°±1
4 EA PER WHEEL | TREAD | UHMW POLYMER | MOLDED IN PLACE WITH FABRIC BACKING | -2
4 EA WHEEL | LOOP CORE | Ti-5AL-2.5SN | ANNEALED | -1
QTY REQD | CODE IDENT | PART OR IDENTIFYING NO | NOMENCLATURE OR DESCRIPTION | MATERIAL DESCRIPTION OR NOTE | MATERIAL SPECIFICATION | ZONE | ITEM NO
PARTS LIST
INTERPRET DWG PER
UNLESS OTHERWISE SPECIFIED DIM ARE IN INCHES. TOLERANCES ON:
FRACTIONS = ± 1/16
DECIMALS: .X = ± .1
.XX = ± .03
.XXX = ± .010
ANGLES = ± 2 DEG
NEXT ASSY | USED ON
APPLICATION
CONTR
CCA/CI/FD
DATE 8-3-77
DWN
APVD
APVD
ENGRG
CHKR
APVD
APVD
LOCKHEED MISSILES & SPACE COMPANY, INC
A SUBSIDIARY OF LOCKHEED AIRCRAFT CORPORATION
SUNNYVALE, CALIFORNIA
Fig. 2-23 - Mars Loopwheel Tread
SIZE C | CODE IDENT | DRAWING NO RBD 951 | REV A
SCALE | SHEET

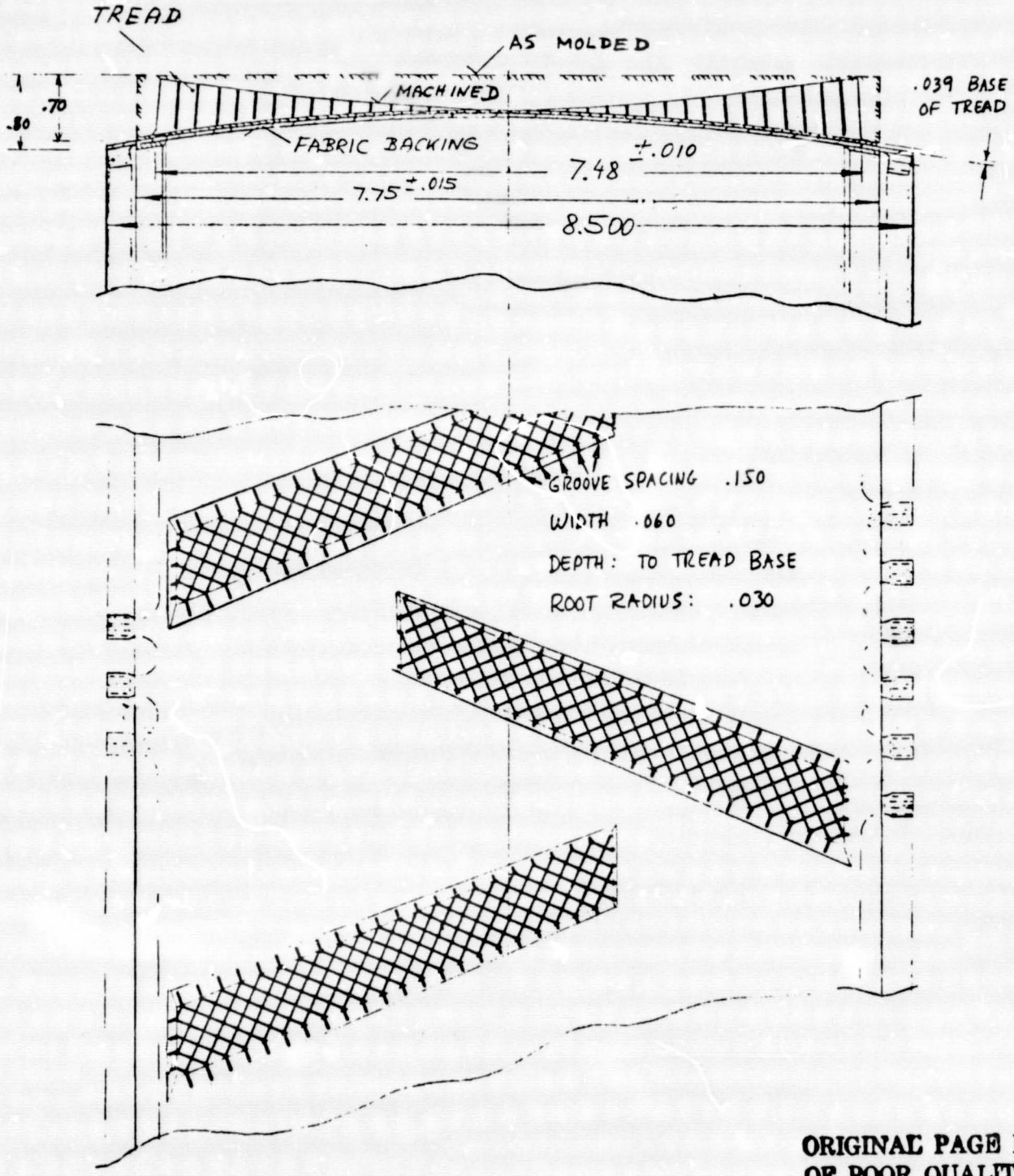

ORIGINAL PAGE IS
OF POOR QUALITY

Fig. 2-24 - Preliminary Tread Details

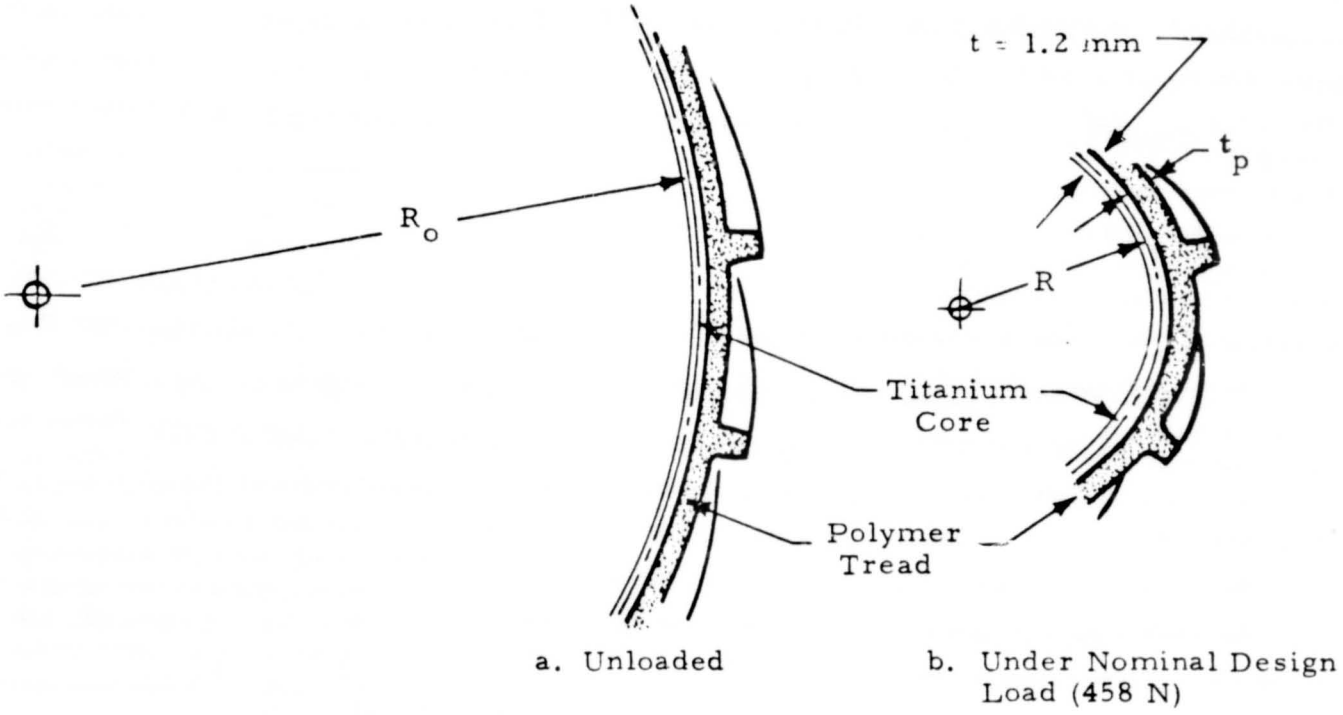

Fig. 2-25 - Loopwheel with Tread in Unloaded and Loaded Configuration

where the conservative assumption was made that the neutral (zero strain) fiber stays at the center of the titanium core. Assuming that the tread is stress free in the unloaded configuration at the average operating temperature, T,

$$T_{\sigma} = \frac{147 + 172}{2} = 160 \text{ K } (-172 \text{ F})$$

the loopwheel flexing under load results in a tensile cyclic stress at the tread's surface (between grousers) with peak

$$\sigma_B = E_{T_{\sigma}} \epsilon_B$$

$$= E_{T_{\sigma}} \left(\frac{t}{2} + t_p\right)\left(\frac{1}{R} - \frac{1}{R_o}\right).$$

For a tread base of thickness t_p = 1.0 mm (0.039 in.), the peak bending stress is

$$\sigma_B = 1724\ (0.6 + 1)\left(\frac{1}{107} - \frac{1}{363}\right) = 18.2 \text{ MN/m}^2 \text{ (2.64 ksi)}.$$

This stress level is already within 83% of the fatigue strength at room temperature given in Fig. 2-16 for 500 km range and within 28% of the yield strength at the average Martian operating temperature given in Fig. 2-15. Although cracks in the tread are not expected to degrade loopwheel performance in any way, they could eventually lead to peeling or chunking of pieces of tread thus exposing the titanium core to rock and soil abrasion and surface damage. Tread design, development and testing is therefore recommended as an important technology area.

Potential improvements in tread fatigue life can be expected from any one or more of the following development efforts:

- Fiber reinforcement of tread material
- Compressive prestressing of tread by elastic expansion of titanium core during tread molding
- Reducing thickness of tread base after establishing typical wear rates over specified range by soil bin tests and sand blasting tests (to simulate dust storms)

- Tailoring of tread material properties to this specific requirement
- Replacement of endless tread firmly bonded to core by an array of overlapping scales, and
- Addition of a strain isolating layer of very soft material (i.e., foam) between core and tread.

The grousers in the present point design as illustrated in Fig. 2-24 are finely grooved with well rounded roots to improve low temperature flexing and reduce weight and stress concentrations at the grouser roots. The narrow width of these grooves and their orientation under approximately $\pm$ 45 deg should not degrade traction in any type of terrain. The total mass of the UHMW polymer tread illustrated in Fig. 2-24 with 1 mm base and 38 grousers per loopwheel of 18.8 cm^3 volume each amounts to

$$m_{tread} = 0.94\ g/cm^3 \times 1160\ cm^3 = 1090\ g$$

per loopwheel.

2.6.3 Preliminary Design of Loopwheel Truck and Drive Sprocket Assembly

2.6.3.1 Truck Design

After the loopwheel loads and major dimensions were established, a preliminary truck design was performed. The main design objectives were:

- Compact overall size for ease of stowage and minimum interference with main chassis during steering and pitching maneuvers
- Minimum open access between loopwheel and truck to minimize the ingestion of rocks and soil during steering and traversing of slopes
- Safe rock and soil removal concept as an integral part of the truck design
- Maximum useful stowage volume, and
- Light weight.

A layout and cross-sectional view of the preliminary truck design is shown in Fig. 2-26.

A riveted sheet metal box forms the main load carrying structure. It is made up of the following major parts:

(2-0), (2-1) Outer and Inner Side Panels with up to Two Windows for Payload Installation

(3) Rear Wall

(4) Top and Front Panel

(5) Bottom Panel

(6) Front Chute for Rock Removal in Reverse Driving

(7) Rear Chute for Rock Removal in Forward Driving, and

(8) Stringer for Reinforcement of Fork Attachment Points.

The front sprocket and front load roller assembly are mounted on swing arms which are pivotally attached to the upper front corners of the side panels. For high-speed terrestrial loopwheel suspensions as shown in Fig. 1-3, a rotary shock absorber is an integral part of the swing arm bearings. Due to the low speed of the Mars rover, no shock absorbers have been included in the present configuration. A conservative weight estimate for the truck, including two load rollers but without sprockets based on 0.030 in. aluminum for all minimum gauge panels and as face sheets for the two swing arms with honeycomb core is 2.63 kg.

2.6.3.2 Stabilization System Design

For high resolution imagery, precision antenna and instrument operation during science stops, a stabilization system (13) has been incorporated in the truck design consisting of an actuator (geared electric motor) and a 7.5 cm long lever with polymer lined roller located at the center of the bottom panel (5). The actuator would be recessed inside a well.

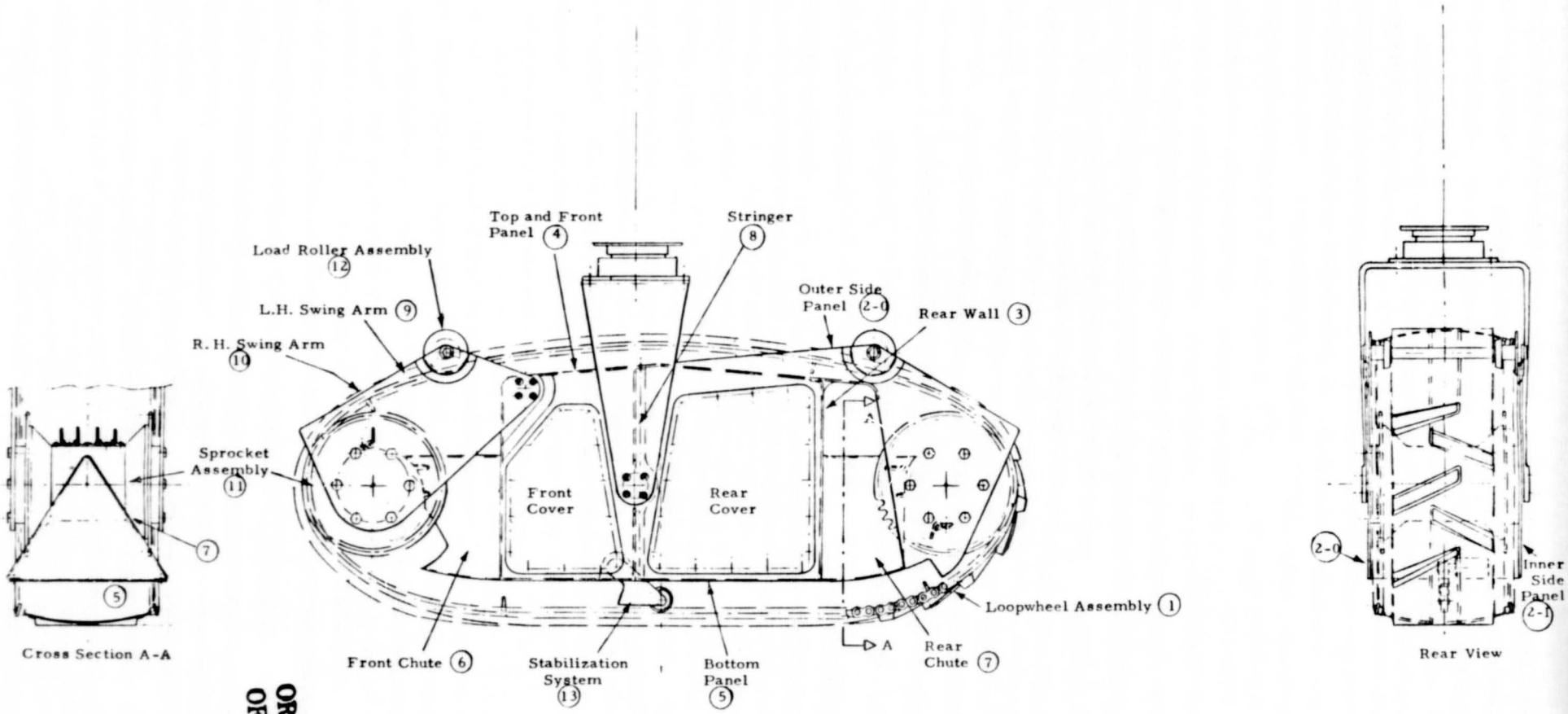

Fig. 2-26 - Preliminary Loopwheel Truck Design

The stabilization system would perform two major functions:

1. Full-Down Position (lever approximately normal to ground)
   a. Provide rigid rover support during science stops by eliminating spring compliance of loopwheels.
   b. Provide maximum access between truck bottom and loopwheels for inspection by camera (and manipulator-held mirror, if necessary) and for rock removal by manipulator in emergency situations not manageable by the normal rock removal procedure described in Section 3.2.

2. Full-Up Position (as shown in Fig. 2-26)

   Roller provides hard stop for loopwheel spring deflection under loads 10% or more above nominal load as encountered in load transfer during slope climbing or descending.

An existing Mars-qualified gear-motor as used in the manipulator joints could actuate the stabilization system thus reducing the impact on development and flight unit cost.

The estimated mass of the total stabilization system including a 4 N-m joint drive motor is 380 g.

2.6.3.3 Sprocket Drive Torque and Power Requirements

The NASA-sponsored performance tests at the U.S. Army Engineer Waterways Experiment Station (WES, Ref. 7) provide a reliable aid in predicting maximum torque and power requirements for sizing the drive system, since actual torque delivered to the sprockets by the gear motor output shafts was measured during the performance tests in lunar soil simulant.

The results plotted in normalized form in Fig. 2-27 were obtained in loose, air dry Lunar Soil Simulant (LSS 1) for a 160 cm long loopwheel at contact pressures of the order 0.275 N/cm^2 (0.4 psi). This compares with $p = 0.39\ N/cm^2$ (0.565 psi) nominal pressure selected for the present point design. This 30% lower contact pressure and the somewhat higher bearing strength of the LSS 1 soil compared with the Martian Loess Engineering

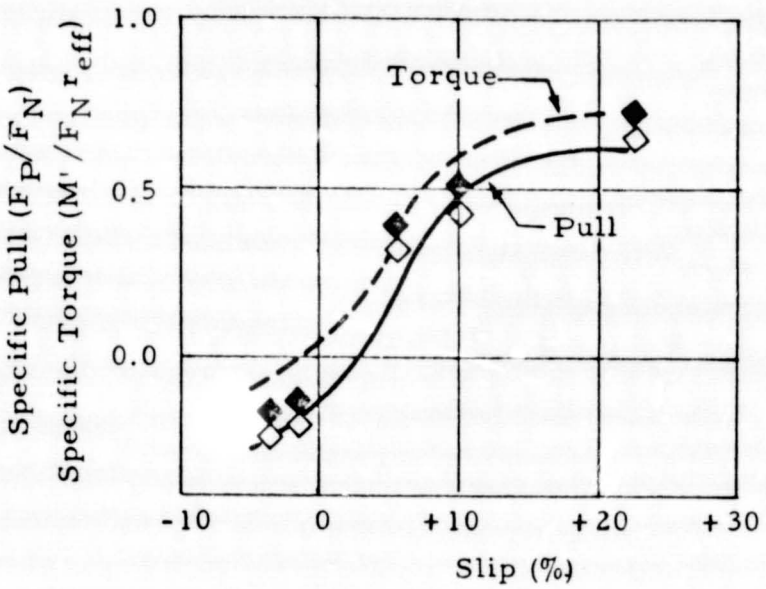

Open Symbols: Pull
Closed Symbols: Torque

a. Pull and Torque Coefficients as Functions of Slip

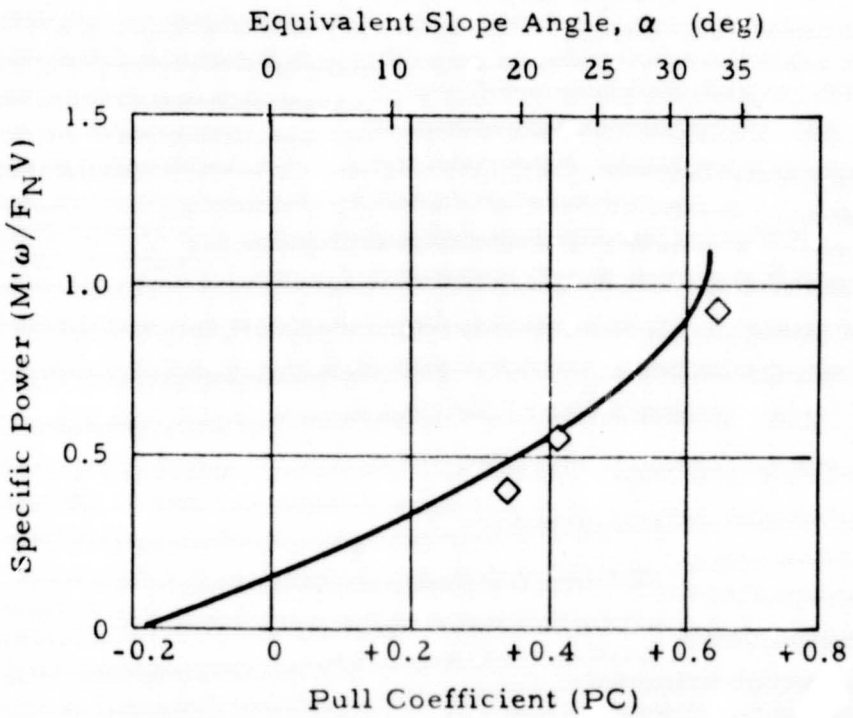

b. Power Number as Function of Pull Coefficient and Equivalent Slope Angle

Fig. 2-27 - Performance Relations from Constant-Slip Tests at WES (Ref. 7), Free-Pitch Mode, Soil Condition LSS1, Drum rpm ≈ 33, W = 565 N

Model of Fig. 2-10 require an upward adjustment of the measured torque characteristics.

A 33% upward adjustment of torque and power levels was selected to obtain conservative values.

From Fig. 2-27a the maximum specific torque $M'/F_N r_{eff}$ measured for a 25-deg slope (or $P/W_N = \tan\alpha = 0.466$) was

$$\frac{M'_{25}}{F_N r_{eff}} = 0.565$$

where M'_{25} is the actual torque delivered to the loopwheel by the sprocket(s) as measured by strain gauges at the gear-motor mounts. $F_N = F_W \cos\alpha$ is the loopwheel load normal to the ground and r_{eff} is the effective sprocket radius.

Assuming worst case load transfer for a suspension with roll articulation yields a maximum load per loop $F_N = 940$ N for a 25 deg slope (according to Fig. 2-6). An effective sprocket radius $r_{eff} = 10$ cm results in

$$M'_{25} = 0.565 \times 940 \times 0.1 = 53.1 \text{ Nm}$$

in LSS 1 test soil or

$$M'_{25} = 1.33 \times M_{25} = 70.6 \text{ Nm}$$

in Martian Loess representing the maximum output torque necessary to drive one loopwheel.

The measured power required to drive the sprockets per N load and per m/sec speed traveled is expressed by the specific power which can be read off Fig. 2-27b for a 25 degree slope:

$$\frac{N'_{25}}{F_N V} = 0.65 \frac{W}{N \; m/sec} .$$

For the present design this leads to a mobility power requirement at the gearhead/sprocket interface

$$N'_{25} = 0.65 \, F_N V$$

$$= 0.65 \, F_W \cos\alpha \; V.$$

For the predicted maximum load per loopwheel of 940 N and a speed of 150 m/hr the mobility power in LSS1-type soil delivered to the sprocket would be

$$N'_{25} = 0.65 \times 940 \; (\cos 25^{\circ}) \; 0.04167$$

$$= 23.1 \text{ W}.$$

Again, assuming a 33% increase in Martian Loess, the maximum sprocket drive power per loopwheel is

$$N'_{25_{\sigma}} = 30.7 \text{ W}.$$

For an efficiency of a brushless motor/gearhead drive unit of

$$\eta_{m/g} = 0.4$$

the maximum electrical input power on 25 degree slopes for the loopwheel carrying the highest load is

$$N_{25_{\sigma}} = \frac{N'_{25}}{\eta_{m/g}} = 76.8 \text{ W}$$

or 38.4 W per sprocket assembly assuming both sprockets are driven and a maximum output torque requirement per sprocket of

$$M_{25_{\sigma}} = 35.3 \text{ Nm}.$$

The maximum drive torque requirements, M_{σ}, during obstacle climbing can be predicted for loopwheel suspensions by:

$$M_{\sqsubset} = \frac{\mu(1 + \mu)}{1 + \mu^2} r_{eff} F_M$$

where μ is the coefficient of friction between loopwheel tread and ground, and F_M is the maximum load per loopwheel. Assuming a 25 deg pitch attitude of the rover chassis after the front loops have climbed a step obstacle, the load transfer to the rear loops is, according to Fig. 2-6 (for a suspension with roll articulation),

$$F_M = 650 \text{ N.}$$

The highest (worst case) coefficient of friction estimated at the Viking I site (Ref. 4) is

$$\mu = 0.65.$$

With $r_{eff} = 0.1$ m the maximum drive torque per loopwheel for climbing a step obstacle then becomes

$$M_{\sqsubset} = \frac{0.65(1.65)}{1.4225} 0.1 \times 650 = 49 \text{ Nm}$$

or 24.5 Nm per drive sprocket which is less than the maximum drive torque for climbing 25 deg slopes at 45 deg azimuth.

2.6.3.4 Sprocket Assembly Design

A preliminary layout of a drive sprocket assembly is shown in Fig. 2-28. The stator of a brushless motor (1) (Model 1903220 Bendix, 32 poles, dual-speed resolver transmitter for commutation, 35 W input power, 2.3 Nm stall torque) is mounted to the left half of the housing (5). A geared parking brake (2) and the commutator are located to the left of the motor. The parking brake is engaged by springs while the magnet is not energized and releases by the magnet under current. A high efficiency planetary roller gearhead (3) is housed in the right hand half of the housing.

A prototype unit of this type had been developed and successfully tested for NASA as a backup LRV component (Ref. 17). The output gear is connected to the sprocket rim (7) by axial pins which can be disengaged by a solenoid-

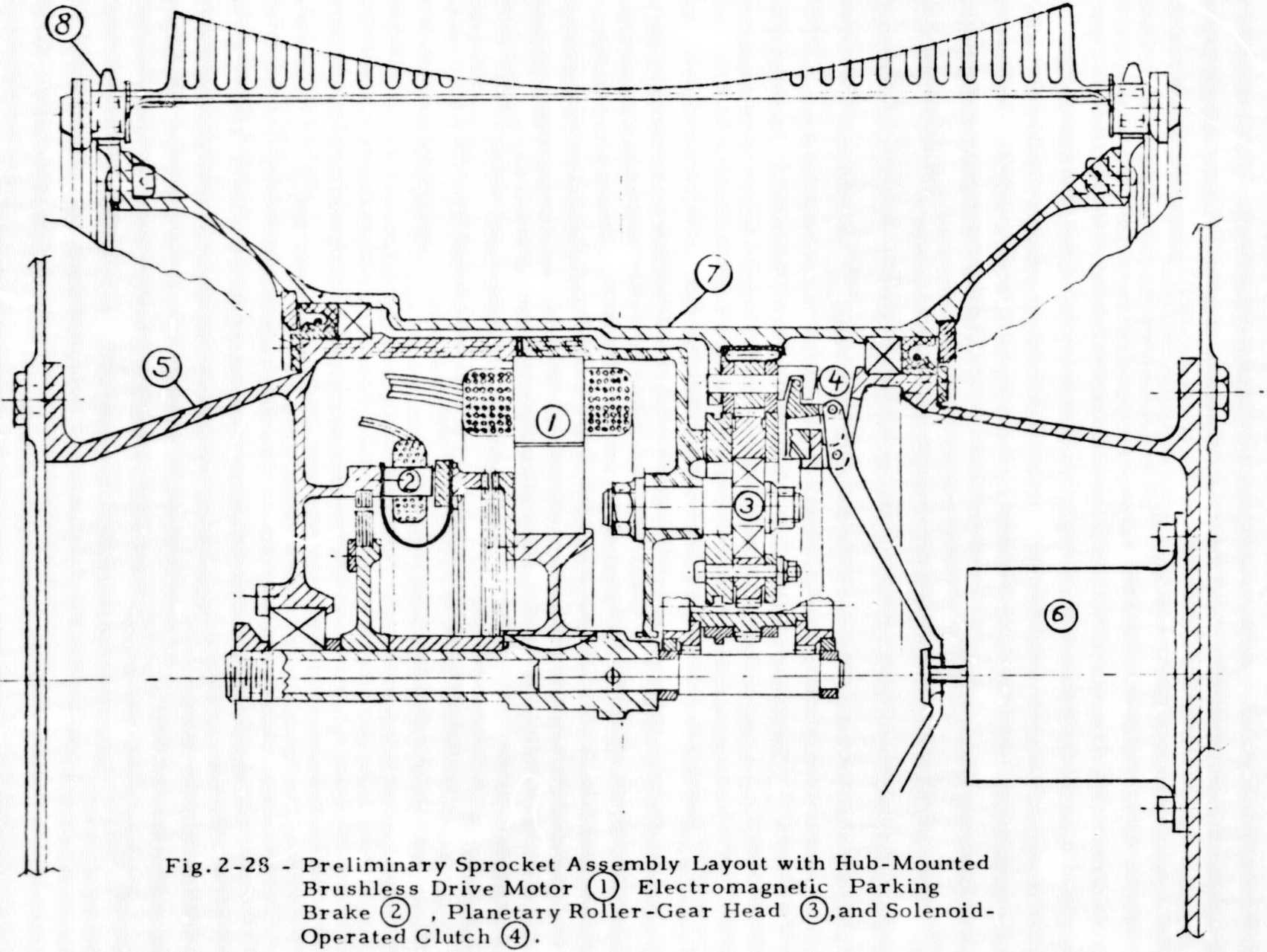

Fig. 2-28 - Preliminary Sprocket Assembly Layout with Hub-Mounted Brushless Drive Motor (1) Electromagnetic Parking Brake (2), Planetary Roller-Gear Head (3), and Solenoid-Operated Clutch (4).

operated clutch (4) in case of motor or gearhead trouble or for motor checkout purposes. The clutch would be kept by springs (not shown) in either engaged or disengaged position. The solenoid (6) would therefore require power only for changing the state of the clutch.

The preferred material for housing (5) and sprocket rim (7) is a lightweight beryllium alloy such as Be-38 Aℓ (density 2.08 g/cm^3).

The two sprocket rings (8) which engage the roller chain-type loopwheel edges are made of titanium with a wear resistant surface coating of hardened steel.

Dry lubrication has been identified as the only safe lubricant in the Martian temperature environment. The limitations imposed by the lubricant on the total number of revolutions of the first mesh in the gear train must be taken into account when the gear ratio and motor size are defined in more detail.

The total mass of the present preliminary drive sprocket assembly design based on a 30:1 gear ratio is 3250 g.

2.6.4 Mobility System Mass Summary

The total mass of the rover mobility system, including four loopwheel truck assemblies with two drive sprockets per carriage, four treaded loopwheel assemblies with all hardware necessary for permanent sprocket engagement, and four stabilization systems is summarized in Table 6. Forks, pitch bearings, cabling and steering actuators are not included.

Table 6

ROVER MOBILITY SYSTEM MASS SUMMARY

Component	Number per Rover	Mass Per Rover (kg)
Loopwheel Core (with Roller Mounts)	4	10.70
Chain Link, Roller, Seal, Fastener	4 sets	3.53
Tread	4	4.36
Truck	4	10.52
Stabilization System	4	1.52
Drive Sprocket Assembly	8	26.00
Total Rover Mobility System Mass		56.63

Section 3

LOOPWHEEL MOBILITY SYSTEM PERFORMANCE PREDICTION

3.1 ROCK AND ROUGH TERRAIN HAZARDS

3.1.1 Singular Rocks and Step Obstacles

The loopwheel's long footprint and inherent bending stiffness in the longitudinal direction make this suspension ideally suited to drive over singular obstacles such as rocks with minimum disturbance to vehicle attitude and with minimum increase in drive motor currents. The critical phases during negotiation of a singular (step-up-step-down) obstacle are shown in the photographs of recent dynamometer tests in Fig. 3-1. The free pitch articulation of all four rover traction elements will equalize spring deflections of the loopwheels and maintain uniform clearance between loopwheel and the bottom of the truck. The vehicle's gradual, near linear rise and fall of the center of mass during singular rock negotiation will be reflected in an equally gradual up-and-down ramping of the motor currents.

The maximum height of singular rocks which can be overcome can be estimated on the basis of obstacle tests performed with a three-loopwheel supported rover model built for NASA (Ref. 18). The vehicle climbed the following obstacles with all loopwheels free in pitch within $\pm$ 45 deg:

Direction of Travel	Step Obstacle Height Climbed (Ref. 18)
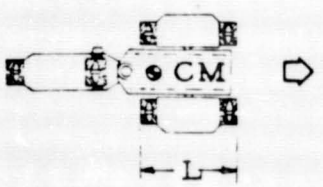	0.85 L
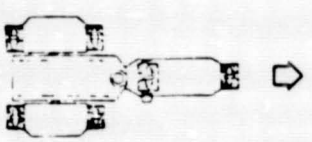	0.64 L

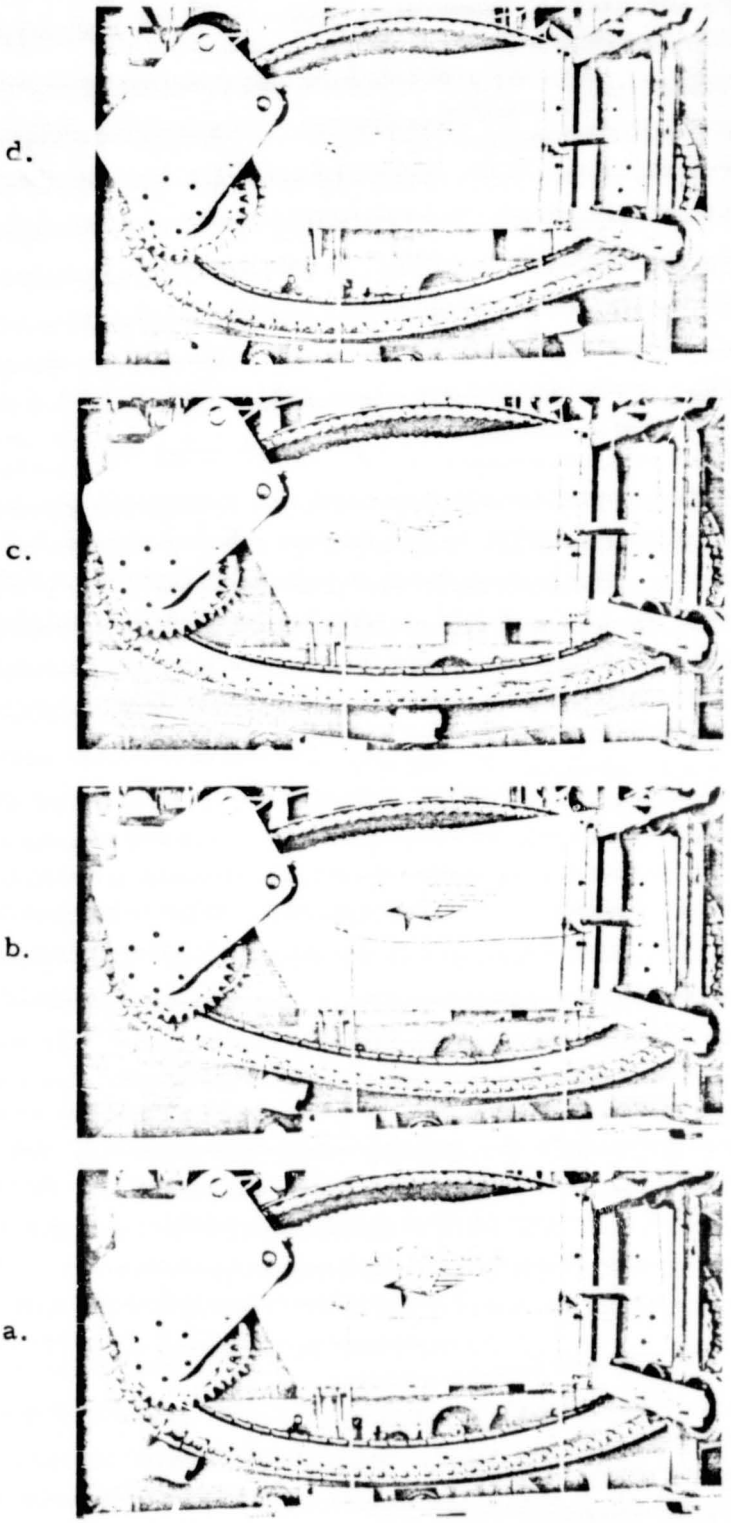

ORIGINAL PAGE IS
OF POOR QUALITY

Fig. 3-1 - Loopwheel Test Unit of 1.27 m Length During Singular Obstacle Negotiation on Moving Belt Dynamometer (Ref. 1). The Loopwheel's Stiff Footprint Results in Smooth Gradual Ascent (a, b) and Descent (d) of Vehicle Without Buckling During Point Load at Center (c). Loopwheel Truck Was Locked in Pitch.

The tests demonstrated that the center-of-mass location with respect to the loopwheels strongly affects obstacle climbing. Since the present four-loopwheel rover design has a well centered center-of-mass location, the predicted maximum obstacle height is

$$H_m = \frac{0.85 + 0.64}{2} L = 0.74\, L.$$

For L = 104 cm, the predicted rock size which can be climbed by the rover is at least

$$H_{Rock} = 77 \text{ cm } (30.3 \text{ in.})$$

which is the step obstacle capability provided that sufficient friction exists under the loopwheels.

3.1.2 Slope Climbing

The NASA-sponsored tests of a 1.6 m long titanium loopwheel test unit at WES (Ref. 7) provide a reliable source to estimate the rover's slope climbing capability.

In the softest test soil condition (LSS1) and with the loopwheel truck free in pitch, the maximum slopes climbed were in the range of

$$30 \text{ deg} \leq \alpha_{max} \leq 33 \text{ deg}$$

as can be seen in the test results of Fig. 2-27b. On compact test soil (LSS5) of higher bearing strength, maximum slope angles negotiated were

$$34 \text{ deg} \leq \alpha_{max} \leq 36.5 \text{ deg}.$$

The slope test set up is shown in Fig. 3-2. The expected very low bearing strength of Martian loess may reduce slope climbing capability at tolerable sinkage levels in loess regions to $\alpha_{max} = 25$ deg.

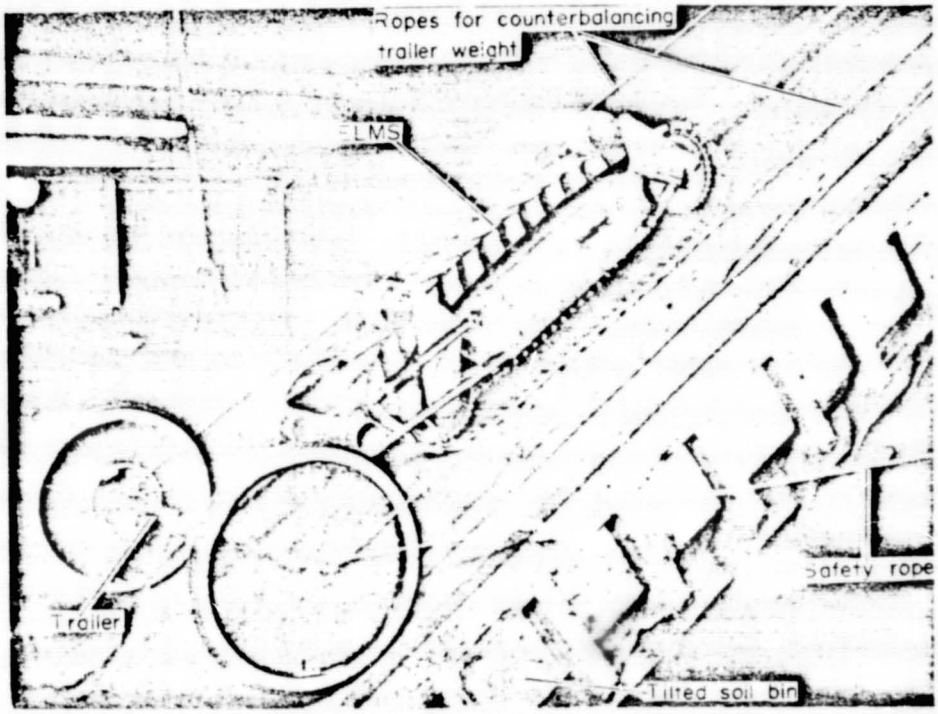

Fig. 3-2 - Slope Climbing Tests of 1.6 m Loopwheel Performed for NASA at WES (Ref. 7) Demonstrated 84% Improvement in Loose Soil (LSS1) and Between 84 and 100% Improvement in Compact Soil (LSS5, Pictured) Compared with LRV Wire Mesh Wheels Tested in the Same Soil and Facility

These estimates can be considered to be conservative since they are based on single loopwheel tests and therefore do not include the gains in traction and propulsive efficiency when rear loopwheels follow the rut of the front loops as demonstrated by the test data in Table 4.

3.1.3 Side Slope Traverses

The maximum side loads identified in Section 2.1 must be safely transmitted from the loopwheels to the chassis without sprocket/loopwheel disengagement.

For design purposes a worst case side load/normal load ratio

$$F_S/F_N = 0.88$$

has been established for safe traverses of 25 deg side slopes and simultaneous scuff steering.

For evaluation and optimization of side load transfer in loopwheel suspensions early in the development Lockheed-Huntsville recently modified its loopwheel dynamometer for realistic laboratory testing of loopwheels under combined vertical and side loads at design speed. Systematic side load tests of the experimental unit shown in Fig. 1-3 were just completed (Fig. 3-3). It was demonstrated that side load/normal load ratios

$$F_S/F_N = 0.95$$

can be safely transmitted without sprocket disengagement if the side load specifications are accounted for during the design of the swing arm/load roller/sprocket configuration.

The specified side load requirements for the present rover point design can therefore be met without difficulty. In the case of unpredictable

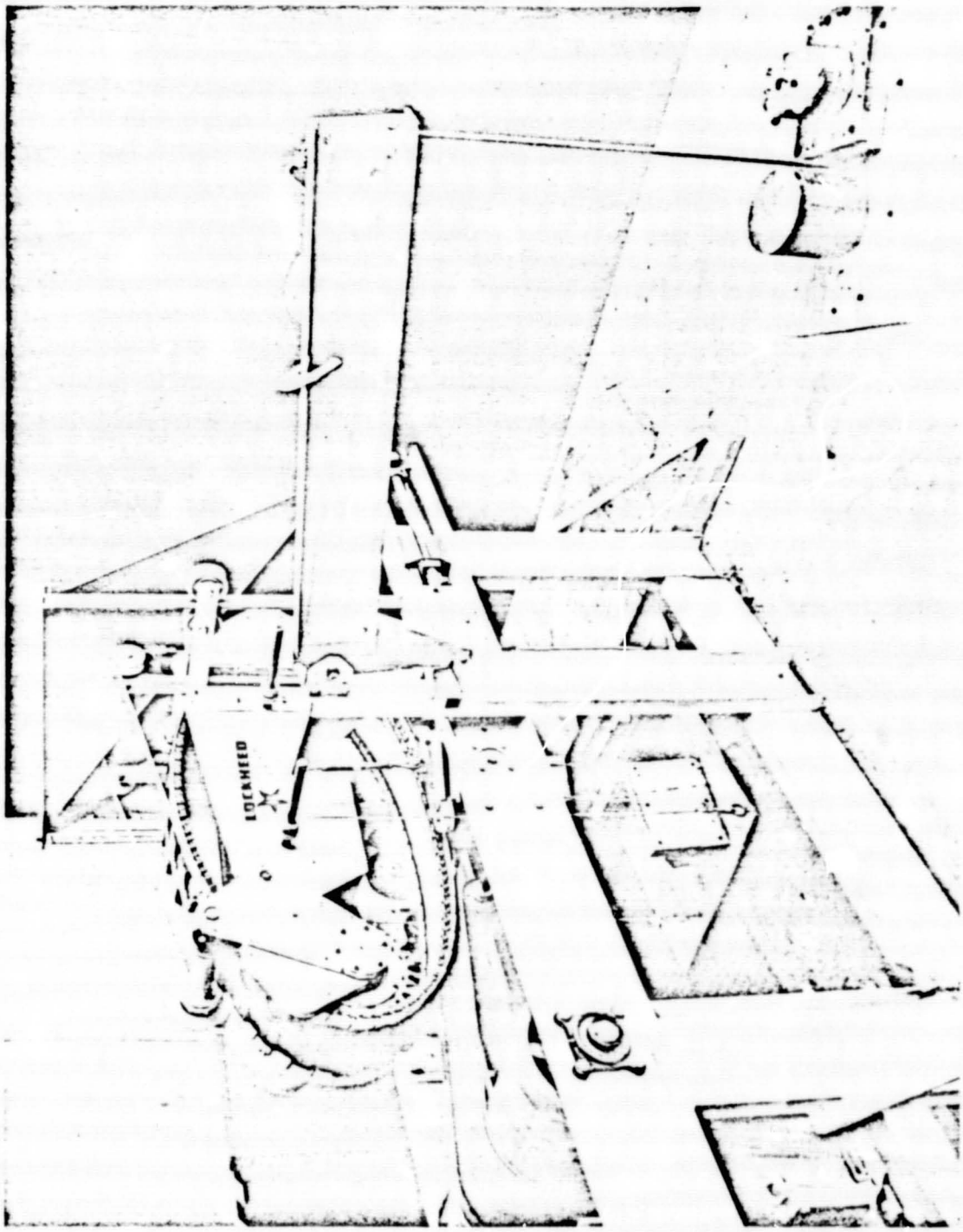

Fig. 3-3 - In Recent Dynamometer Tests Under Combined Side Loads and Vertical Loads the Predicted Worst Case Loads Due to Scuff Steering on Maximum Side Slopes Were Exceeded Without Sprocket Disengagement (Ref. 1)

ORIGINAL PAGE IS
OF POOR QUALITY

excessive side loads extensions of the swing arms and the truck side walls in the fore and aft direction will keep the loopwheel aligned with the sprocket during temporary disengagement and thus assure safe reengagement immediately after the side load falls below the critical level. This automatic peak side load accommodation has also been demonstrated repeatedly during the recent side load test phase.

3.1.4 Removal of Ingested Rocks and Soil

One of the important design goals in laying out the loopwheel suspension system was to minimize the area of openings which are subjected to rock and soil ingestion. The clearance between the loopwheel' s lower section and the truck is therefore kept under 4 cm. This clearance is necessary to allow for loopwheel twisting on uneven ground without interference with the truck bottom.

As illustrated in Fig. 3-4, soil and rocks which are small enough to be ingested are conveyed upward at the rear section of the loopwheel by loopwheel-mounted flexible strakes. Similar arrays of strakes or metal wire rakes are installed radially on the sprocket rims to support the lifting of the ingested material around the sprocket rim to be finally dumped on a two-sided chute which deflects the material to the outside of the loopwheel' s envelope.

If a rock of very peculiar shape or a large accumulation of rocks and/or soil should cause jamming of a loopwheel, the following automatic cleaning procedure is proposed:

1. The jammed loopwheel is identified by a check of all four tachometer and motor current readings.
2. The roll articulation between front and rear suspension is locked.
3. The stabilization systems of the healthy loopwheels are deployed downward.
4. A computation is made if the attitude change during deployment of the stabilization systems has lifted the jammed loopwheel off the ground.

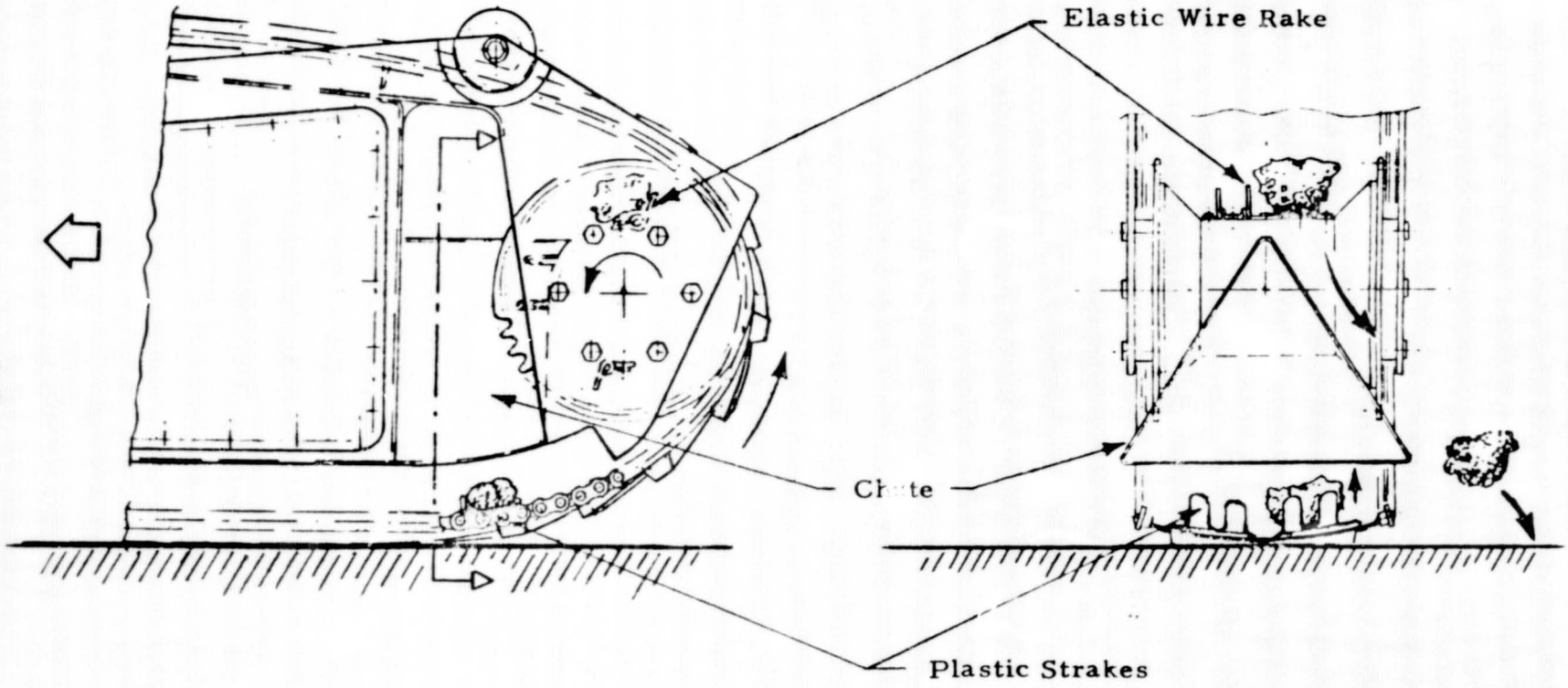

Fig. 3-4 - Candidate Concept for Removal of Ingested Rocks and Soil Using Loopwheel-Mounted Strakes Which Lift Material Above Sprocket to be Dumped by the Chute

5a. If "Yes," the jacked up loopwheel is run in opposite direction of the direction which led to jamming for at least two loop revolutions or until motor current and tachometer readings are smooth.

b. If "No" (jammed loopwheel not likely to be off the ground), the manipulator is deployed and pushed down into the ground near the jammed loop to tilt the rover until the jammed loop clears the ground.

6. Loopwheel is cleaned as in 5a.

This housekeeping sequence should not require any earth link under normal circumstances and should be completed within approximately four to six minutes.

This and alternate concepts for rock removal and for cleaning operations should be verified and refined early in the rover development by a functional engineering test vehicle.

3.2 DUST AND WIND EFFECTS

The mission duration requirement on the Rover is to perform for one Martian year after landing. It must therefore be designed to survive at least one of the yearly global dust storms. In addition to this yearly storm season, great dust storms may be encountered. The last great storm was observed in 1971 which shrouded the entire planet. A third category is localized storms.

Observations of the sky at the Viking 1 site (Ref. 19) indicate that the mean radius of particles suspended in the atmosphere is 1 μm which is comparable to values deduced from observations of dust particles present in the last great dust storm of 1971.

Even outside the storm season, local gusts have been measured as strong as 15.9 m/sec (Ref. 4).

Of all the mobility system hardware the sprocket assemblies housing the drive motors and gear heads have been identified as the most vulnerable

subsystems which will require carefully developed dust seals.

The loopwheels are well protected from abrasive wind effects by the outer tread which is made of the highly abrasion-resistant UHMW polymer. Likewise, the chain links and rollers must be made of wear-resistant materials of high surface hardness and possibly special coatings to limit wear in operation due to sprocket engagement as well as abrasive wear from dust storms to tolerable levels.

Further design efforts must be directed toward protecting the roller and chain link bearing surfaces against dust depositions. A preliminary design of the sprocket/loopwheel interface is shown in Fig. 3-5. The roller bearing surface is sealed from dust by two O-rings whereas two Belleville spring washers seal the holes in the chain links to preserve the dry lubricant in the bearing areas. Similar roller chain sealing concepts are used successfully in extending the life of competition "enduro" motorcycles operating in dirt and dust. In addition to dust-conscious design efforts operational procedures must be defined which maximize the probability of achieving the specified range and of surviving a major dust storm. Such procedures should include cleaning of all four loopwheels following the jack-up concept described in Section 3.1 in the waning phase of a dust storm whenever there are indications of substantial deposition of sediment inside the loopwheels.

A precaution against getting "buried" during a major dynamic event would be to head the rover precisely into the wind as soon as a specified wind velocity is exceeded and move at a very low speed in the order of 10 m/hr throughout the storm. Depending upon the terrain, forward or backward motion can be selected to prevent excessive drift formation around the rover. The heading into the wind (or precisely downwind) provides maximum protection to the loopwheel drive systems which are thus shadowed by the loopwheels.

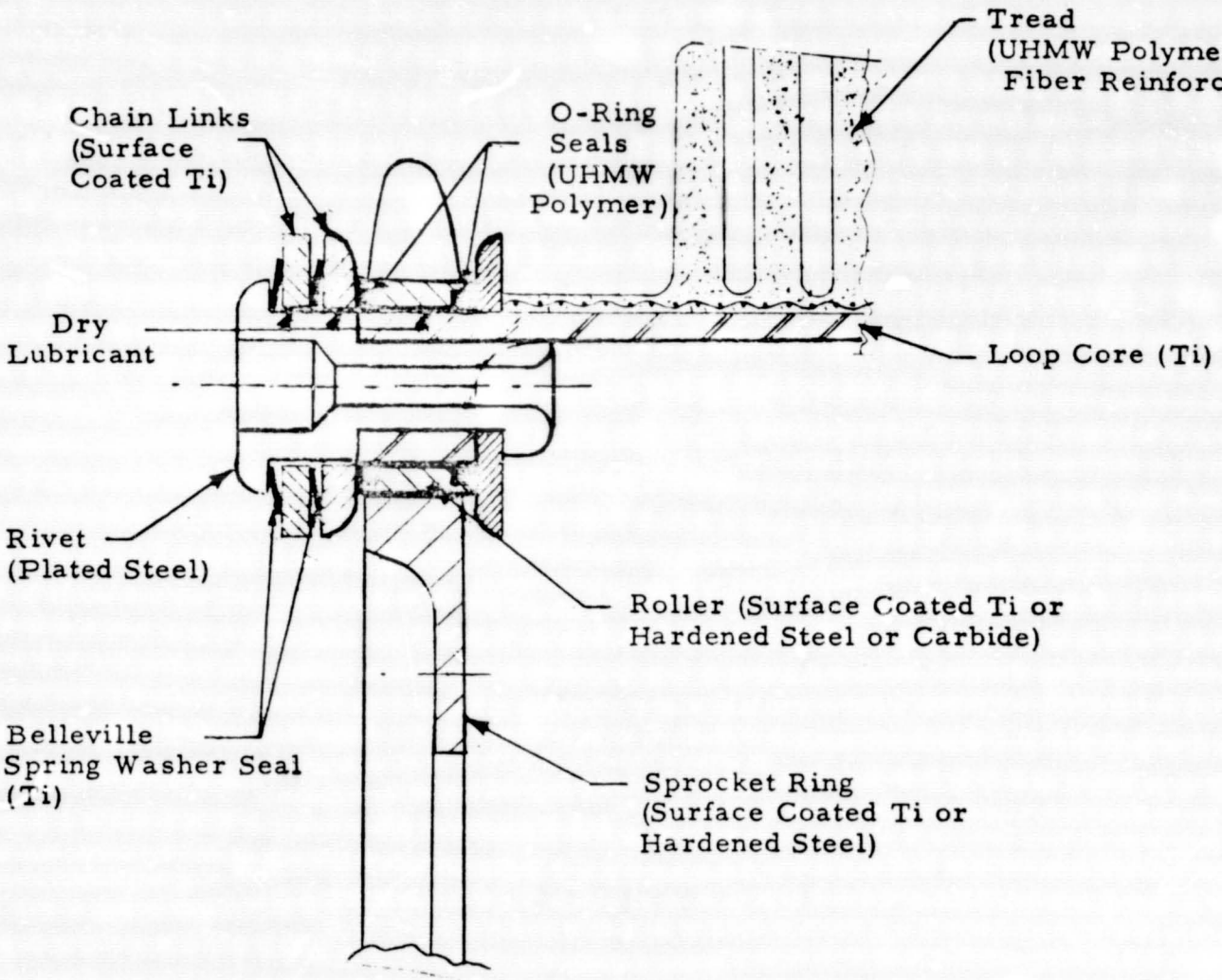

Fig. 3-5 - Details of Sprocket/Loopwheel Engagement with Dust Seals to Protect Chain Link and Roller Bearing Surfaces

Early in the rover development, the sealing concepts for the drive motor housings as well as those proposed for the load roller bearings and the sprocket/loopwheel interface should be validated by abrasion tests in appropriate sand-blasting facilities under controlled conditions which can be correlated to Martian dust storm intensities.

3.3 LOOPWHEEL SURFACE DAMAGE EFFECTS

An important goal in the design of the loopwheel core and tread system is the protection of the cyclically stressed titanium core from nicks, scratches and abrasion by the outer tread of UHMW polymer.

Strict precautions should be taken in the design and development of the tread and the way it is fastened to the loop core so that the loop core is nowhere exposed to direct contact with the ground throughout the design life of the rover. However, due to the vital importance of the structural integrity of the four loopwheel cores for mission success it has been assumed that surface damage of the loop cores will occur early in the mission by some unpredictable event whereby the protective skin provided by the tread is lost.

As a worst case surface damage, a deep scratch of the following dimensions was assumed to reach across the full width of the loopwheel core as illustrated in Fig. 3-6:

Depth of Scratch: $b = 4r$, where r = radius at root

and net undamaged thickness

$$h = r/0.02$$

$$= 50\,r.$$

These were the most severe values in the chart of stress concentration factors from Ref. 20. The resulting stress concentration factor for this severe notch is

$$K_t = 4.5.$$

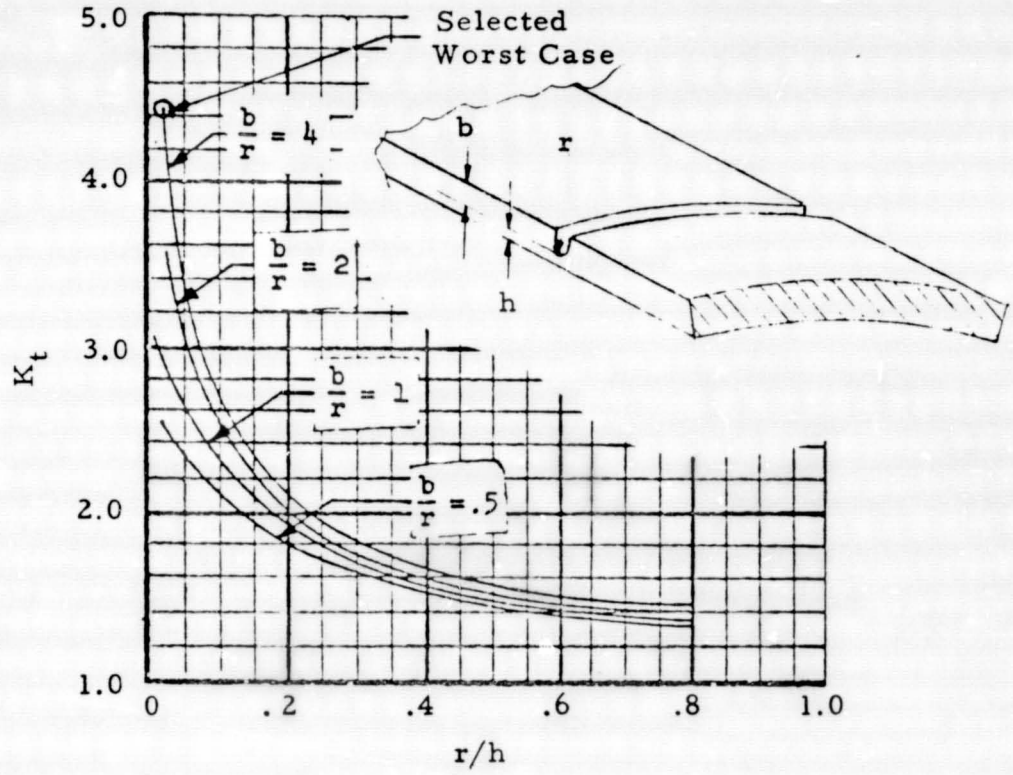

Fig. 3-6 - Stress Concentration Factor Due to Transverse Notch Across Entire Loop Core, Worst Case Surface Damage Assumed: b/r = 4.5; r/h = 0.02 (highest value in chart from Ref. 20)

This value is also in agreement with Lockheed's life assurance manual (Ref. 21) for fatigue critical titanium structures in the absence of specific fatigue test data.

As an additional precaution, it was assumed that during the operation of the notched loop core, additional knicks, scratches or abrasion occur in the notch area. A damage stress concentration factor

$$K_d = 1.1$$

is recommended in Ref. 21 to account for such effects.

These two stress concentrations then result in the following allowable stress in the damaged loop core

$$\sigma_A = \frac{\sigma_{500_{\sigma'}}}{K_t K_d}$$

$$= \frac{671}{4.5 \times 1.1} = 136 \text{ MN/m}^2 \text{ (19.7 ksi)}$$

where $\sigma_{500_{\sigma'}}$ is the predicted fatigue strength of the unnotched material at the Martian surface temperatures derived in Section 2.3.

Comparing this allowable stress with the predicted operating stresses of the present loop core design in Section 2.6.1, namely

$$\sigma_{T_{max}} = 127.8 \text{ MN/m}^2 \text{ (18.5 ksi)}$$

$$\sigma_{C_{max}} = 115.8 \text{ MN/m}^2 \text{ (16.8 ksi)}$$

shows that the present design is safe against fatigue failure for a 500 km range in the Martian temperature environment, even with severe surface damage suffered at the start of the mission.

This surface damage analysis should be refined as material characteristics of surface notched specimens at low temperature become available.

Existing fracture toughness data typically were generated with thick specimens, positive stress ratios and at room temperature. However, in the absence of representative fatigue test data for surface flawed specimens, the above preliminary analysis can be considered to be conservative.

Section 4
CONCLUSIONS AND RECOMMENDATIONS

Loopwheel traction elements have been designed for JPL's Mars Rover point design of May 1977. Conservative assumptions were used concerning the bearing strength of fine Martian soil in sizing the loopwheels.

The effects of the low temperature environment and of potential surface damage by rocks or abrasion were included in the design and analysis of fatigue critical components.

Design charts were prepared for loopwheel sizing as an aid in future refinements and modifications as mission planning matures.

Of four steering concepts evaluated, double Ackermann steering was found to provide the highest probability of mission success and the highest degree of failure tolerance.

Free roll articulation between front and rear loopwheel suspension is proposed for improved mobility and for limiting load transfer from uphill to downhill loopwheels during slope climbing.

The total mobility system mass is approximately 11% over JPL's April 1977 estimate (56.6 vs 49.8 kg). However, large additional payload volume (0.103 m^3) has been incorporated into the loopwheel truck design which represents over 20% of the present size of the rover equipment compartment. The close proximity of these payload bays to the ground make the installation of deployable science payload attractive. Any equipment moved from the rover equipment compartment into these truck bays improves stability, obstacle and slope climbing ability by lowering the vehicle's c.g. Also, the rover then requires less space for stowage inside the aeroshell.

The following technology areas are recommended for continued support since they promise the highest return in future development risk reduction and development cost savings:

- Development and validation by full-scale tests of optimum concepts for steering (primary and backup), chassis roll articulation, rock and soil removal, traction element jack-up and self cleaning. (These tasks require a full-scale functional rover model.)
- Low temperature fatigue testing of candidate tread materials and surface flawed titanium core material.
- Process development and verification for the fatigue-proof joining of the plastic tread to titanium loopwheel cores.
- Dust storm proof shaft seal development and verification.

Since autonomous mobility will be a key asset of the next mission to Mars, continued support in these critical areas will provide NASA and the science community with a sound technology base and better understanding of the vast expansion of exploration capability and science return possible with an autonomous high-mobility rover.

Section 5
REFERENCES

1. Trautwein, W., "Loopwheel Suspension System Development — Final Report," Contract DAAE07-76-C-3246, September 1977, to be published by Army Tank Automotive Research & Development Command, Warren, Mich.

2. "Mars Rover Assembly," JPL Drawing No. 10083076, 12 May 1977.

3. "Mars '84 Rover System Point Design Description," Preliminary JPL Memorandum, 7 April 1977.

4. Mutch, T.A., et al., "The Soil of Mars (Viking I)," Science, Vol. 194, 1 October 1976, pp. 91-97.

5. Mutch, T.A., et al., "The Surface of Mars: The View from the Viking 2 Lander," Science, Vol. 194, 17 December 1976, pp. 1277-1283.

6. Green, A.J., and K.-J. Melzer, "Performance of the Boeing-LRV Wheels in a Lunar Soil Simulant; Effect of Wheel Design and Soil," Technical Report M-71-10, Report 1, U.S Army Engineer Waterways Experiment Station, Vicksburg, Miss., December 1971.

7. Melzer, K.-J., and G.D. Swanson, "Performance Evaluation of a Second-Generation Elastic Loop Mobility System," Technical Report M-74-7, U.S. Army Engineer Waterways Experiment Station, Vicksburg, Miss., June 1974.

8. "MARS Engineering Model," NASA Report M75-125-3.

9. Costes, N.C., J.E. Farmer, and E.B. George, "Mobility Performance of the Lunar Roving Vehicle: Terrestrial Studies — Apollo 15 Results," NASA Technical Report No. R-401, 1972, National Aeronautics and Space Administration, Washington, D.C.

10. "Use of Loopwheel Mobility Systems on the Viking '79 Lander," LMSC-HREC D390251, Lockheed Missiles & Space Company, Huntsville, Ala., June 1974.

11. "Viking III Program Mobile Lander Technical Studies," MMC Report S76-44594-001, Martin Marietta Corp., Denver, Colo., January 1977.

12. Campbell, J.E., "Fracture Toughness of High-Strength Alloys at Low Temperature," ASTM STP 556, American Society of Testing and Materials, 1974, pp. 4-21.

13. Tobler, R.L., "Low Temperature Fracture Behavior of a Ti-6Al-4V Alloy," Report NBSIR-76-836, National Bureau of Standards, Boulder, Colo., April 1976.

14. Adsit, N.R., et al., "Flexural Fatigue Testing of Titanium Forging Material in Liquid Hydrogen," ASTM-STP-556, American Society for Testing and Materials, 1974, pp. 44-54.

15. "Abrasion-Resistant 1900 UHMW Polymer," Hercules, Inc., Wilmington, Del.

16. "Flexural Fatigue Evaluation of UHMW 1900 and Competitive Resins," Internal Memorandum RI PTC 723, Hercules, Inc., Polymers Technical Center, Wilmington, Del., November 1970.

17. Seminski, R.B., and G.F. Auclair, "Roller-Gear Drive Development," Final Report ACD 10,104, General Electric Company, Binghamton, N. Y., February 1971.

18. Trautwein, W., "Fabrication and Testing of Elastic Loop Roving Vehicle Models – Summary Report," LMSC-HREC TR D306460-I, Lockheed Missiles & Space Company, Huntsville, Ala., March 1973.

19. Mutch, T.A., et al., "Fine Particles or Mars," Science, Vol. 194, 1 October 1976, pp. 87-91.

20. Peterson, R.E., Stress Concentration Design Factors, First Edition, Wiley, New York, 1953.

21. "Structural Life Assurance Manual," Lockheed-California Company, Revised December 1975.